Bursting regimes in map-based neuron models coupled through fast threshold modulation

Borja Ibarz,[1,][*] Hongjun Cao,[1,2] and Miguel A. F. Sanjuán[1]

[1]*Nonlinear Dynamics and Chaos Group, Departamento de Física, Universidad Rey Juan Carlos,*
Tulipán s/n, 28933 Móstoles, Madrid, Spain

[2]*Department of Mathematics, School of Science, Beijing Jiaotong University, Beijing 100044, People's Republic of China*

A system consisting of two map-based neurons coupled through reciprocal excitatory or inhibitory chemical synapses is discussed. After a brief explanation of the basic mechanism behind generation and synchronization of bursts, parameter space is explored to determine less obvious but biologically meaningful regimes and effects. Among them, we show how excitatory synapses without any delays may induce antiphase synchronization; that a synapse may change its character from excitatory to inhibitory and vice versa by changing its conductance, without any change in reversal potential; and that small variations in the synaptic threshold may result in drastic changes in the synchronization of spikes within bursts. Finally we show how the synchronization effects found in the two-neuron system carry over to larger networks.

PACS number(s): 87.10.−e, 05.45.−a, 84.35.+i

I. INTRODUCTION

Among the topics of interest in theoretical neuroscience, the dynamics of networks of coupled neurons stands out as a very fundamental problem with deep implications for our understanding of the brain. In particular, the collective behavior of neural assemblies, detected as synchronous components in brain signals, has been shown to be correlated with cognitive activities [1] during the normal functioning of the brain, while important brain disorders, such as epilepsy, Parkinson's disease, Alzheimer's disease, schizophrenia, and autism, are linked to abnormal synchronization [2].

The relevance of neural synchronization has prompted a great deal of recent theoretical and computational work on the synchronizing behavior of neuron models, in particular in networks of bursters. Bursting neurons, which respond to steady current injection with repetitive sequences of spikes, make up a variety of important neural and excitable cell systems, including pancreatic β cells in charge of the secretion of insulin [3], the thalamic reticular nucleus responsible for rhythms during sleep [4], areas in the basal ganglia related to motor control [5], and central pattern generators that drive coordinated rhythmic tasks [6]. Nevertheless, the mechanisms leading to collective dynamic patterns and synchronization in such systems are not fully understood.

The dynamics of bursting has been extensively studied and classified for single neuron models [7], and there is no lack of studies about the synchronization regimes in networks of bursters [8], including some by the authors [9,10]. In the present work we study the synchronization between two map-based square bursters coupled through fast threshold modulation (FTM) [11] and show how the behaviors we find affect the dynamics of larger networks. In contrast with our previous work, where by using linear coupling we were able to profit from the power of master stability functions [12] to predict activity patterns, here we use the FTM coupling model, which precludes such linear analysis, but includes biologically relevant coupling parameters (conductance, synaptic threshold, and reversal potential), allowing us to obtain biologically meaningful results about burst and spike synchrony. In particular we show that in this kind of bursters shunting synapses can be made to promote either in-phase or antiphase burst synchronization, depending either on synaptic conductance or cell polarization. This is a phenomenon that differs from other similar results about the dependence of the phase of synchronization on synaptic time scales [13], or about modulating *spike* synchronization regimes [14,15]. We conclude with a discussion on how the modulation of bursting regimes translates into a control of network modes of synchronization.

II. DESCRIPTION OF THE COUPLED MAP-BASED NEURON SYSTEM

We consider a simple network of two identical map-based neurons [16,17] coupled through reciprocal excitatory or inhibitory chemical synapses that follow the fast threshold modulation (FTM) model [18,11]:

$$x_{n+1,1} = F_\alpha(x_{n,1}, y_{n,1} + \beta_{n,1}),$$

$$y_{n+1,1} = y_{n,1} - \eta(x_{n,1} - \sigma),$$

$$x_{n+1,2} = F_\alpha(x_{n,2}, y_{n,2} + \beta_{n,2}),$$

$$y_{n+1,2} = y_{n,2} - \eta(x_{n,2} - \sigma), \qquad (1)$$

where

$$\beta_{n,1} = -g_c H(x_{n,2} - \theta)(x_{n,1} - \nu),$$

$$\beta_{n,2} = -g_c H(x_{n,1} - \theta)(x_{n,2} - \nu).$$

The x variables represent the transmembrane voltage of each neuron, appropriately scaled, whereas the y variables represent slow gating processes. In the β coupling terms, $H(x_{n,i})$ ($i=1,2$) is the Heaviside step function and θ is the presynaptic threshold for chemical synaptic interaction. Thus only

*borja.ibarz@urjc.es

when the presynaptic neuron voltage x is above θ does the postsynaptic neuron receive any external input. This is a useful simplification of the way fast chemical synapses work, and θ is closely related to the sharp voltage response of the presynaptic terminals. The constant ν denotes the reversal potential associated with the synapses, which is defined by the nature of the postsynaptic ionic channels. The synapse will be excitatory if ν is higher and inhibitory if ν is lower than the range of $x_{n,i}$ (the intermediate cases will deserve further discussion later). Parameters α and σ are $O(1)$, while η satisfies $0 < \eta \ll 1$. Parameter $g_c > 0$ denotes the coupling strength of chemical synapses; it is linked to the aggregate of the maximal conductances of the postsynaptic channels.

Due to the smallness of the parameter η, the evolution of $y_{n,i}, (i=1,2)$ is much slower than that of $x_{n,i}, (i=1,2)$. Thus we will refer to $x_{n,i}$ as the fast variables and $y_{n,i}$ as the slow variables, and we will divide the system of Eqs. (1) into two subsystems:

$$x_{n+1,1} = F_\alpha(x_{n,1}, \gamma_1 + \beta_{n,1}),$$

$$x_{n+1,2} = F_\alpha(x_{n,2}, \gamma_2 + \beta_{n,2}), \qquad (2)$$

and

$$y_{n+1,1} = y_{n,1} - \eta(x_{n,1} - \sigma),$$

$$y_{n+1,2} = y_{n,2} - \eta(x_{n,2} - \sigma). \qquad (3)$$

For convenience, we call Eqs. (1) the full system, Eqs. (2) the fast subsystem, and Eqs. (3) the slow subsystem. From now on, whenever we want to stress the role of y as a parameter of the fast subsystem we will refer to it as γ.

The nonlinear function $F_\alpha(x,y)$ is responsible for the generation and reset of spikes. We will use two different forms of $F_\alpha(x,y)$, which will give rise to two different versions of the neuron model. The first one [16], which we will refer to as the chaotic Rulkov model, is given by

$$F_\alpha(x,y) = \frac{\alpha}{1+x^2} + y. \qquad (4)$$

The second one [17], which we will refer to as the nonchaotic Rulkov model, is given by

$$F_\alpha(x,y) = \begin{cases} \dfrac{\alpha}{1-x} + y, & \text{if } x < 0, \\ \alpha + y, & \text{if } 0 \le x < \alpha + y, \\ -1, & \text{if } x \ge \alpha + y. \end{cases} \qquad (5)$$

Observe that variable y enters into $F_\alpha(x,y)$ additively in both cases, except in the threshold-and-reset pieces of the nonchaotic map (see Fig. 1). Thus we may write

$$F_\alpha(x,y) = f_\alpha(x) + y, \qquad (6)$$

and, if we consider y as a parameter γ, $F_\alpha(x,\gamma)$ will represent a return map that is shifted up or down by increasing or decreasing γ. The shape of this map is represented in Fig. 1 for both forms of $F_\alpha(x,\gamma)$. In both maps a pair of fixed points exists for low values of γ that disappear through a saddle-node bifurcation when γ increases. The rationale for
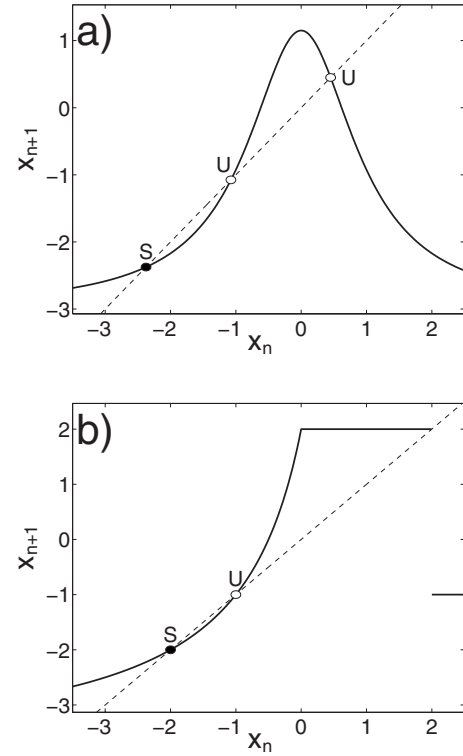

FIG. 1. Return map $F_\alpha(x,\gamma)$ for the fast variable of (a) the chaotic Rulkov model, with $\gamma = -3$ and $\alpha = 4.15$, and (b) the nonchaotic Rulkov model, with $\gamma = -4$ and $\alpha = 6.0$. With these values of α both models are bursters, and the values of γ have been chosen in the region of bistability. S and U denote stable and unstable fixed points, respectively, of the fast map. The shape of the fast maps is the only difference between the two variants of the model, with the consequence that in (a) we get irregular bursts, while in (b) bursts are regular.

the terms chaotic and nonchaotic becomes clear at the sight of the return maps: the first one corresponds to a unimodal map with chaotic orbits, while the second one only presents periodic orbits. A unimodal fast map is a convenient way to introduce unpredictability in the sequence of spikes, but other choices are possible. For example, a similar bursting model is obtained by using a Lorenz-type return map [19], and our results about burst synchronization carry over to it as well in the appropriate range of parameters. Particular choices of the chaotic fast map will affect *spike*, but not *burst* dynamics, which is the main focus of our study.

When $g_c = 0$, Eqs. (1) represent two identical neurons without any coupling. It has been shown [16,20] that the behavior of a single neuron can be predicted by studying the dynamics of the one-dimensional subsystem $x_{n+1} = F_\alpha(x_n, \gamma)$. The key to bursting is the fact that there is a range of values of the bifurcation parameter γ for which there is bistability. This range is defined by two bifurcations: the saddle-node bifurcation γ_{sn} on one side, and, on the other, either the external crisis bifurcation γ_{cr} (in the chaotic model) or the homoclinic bifurcation γ_h (in the nonchaotic model). Both are represented on nullcline diagrams of the full system in Fig. 2.

In the chaotic map [Fig. 2(a)], γ_{cr} is the value of γ where the minimum iterate of x_n (which is the second iterate of the
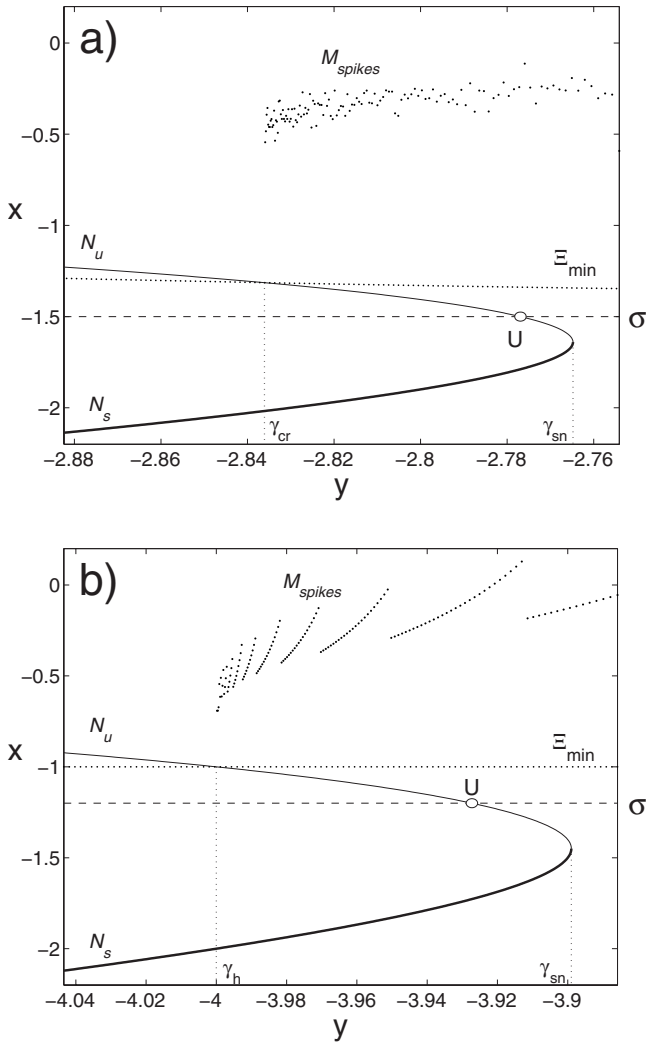
FIG. 2. Nullcline diagrams of the Rulkov models. (a) Chaotic model with $\alpha=4.15$, $\sigma=-1.5$. N_s and N_u are stable and unstable branches of the fast nullcline; $y=\gamma_{sn}$ marks the saddle-node bifurcation of the fast subsystem. The dashed horizontal line is the slow nullcline at $x=\sigma$. The dotted, nearly horizontal line Ξ_{min} represents the second iterate of the critical point $x=0$. γ_{cr} is the value of y of the external crisis bifurcation. M_{spikes} is the manifold of average values of spiking in the fast subsystem at each fixed value of y. (b) Nonchaotic model with $\alpha=6.0$, $\sigma=-1.2$. Same labels as before; now Ξ_{min} is at the reset level $x=-1$ and γ_h marks the homoclinic bifurcation.

FIG. 3. (Color online) Bursting orbit in phase space of (a) the chaotic Rulkov model, with $\alpha=4.15$, $\sigma=-1.2$, and $\eta=0.001$, and (b) the nonchaotic Rulkov model, with $\alpha=6.0$, $\sigma=-1$, and $\eta=0.002$. N_s and N_u denote the stable and unstable branches of fixed points of the fast subsystem, respectively. Ξ_{max} and Ξ_{min} are the maximum and minimum possible iterates of the fast map for each value of y. γ_{cr}, γ_h, and γ_{sn} mark the y values of the external crisis, homoclinic, and saddle-node bifurcations, respectively.

critical point $x=0$) maps onto the unstable middle branch of the curve of fixed points. In the nonchaotic map [Fig. 2(b)], γ_h is the value of γ at the intersection between the unstable branch of the curve of fixed points and the reset level $x=-1$. When $\gamma_{cr} < \gamma < \gamma_{sn}$, or $\gamma_h < \gamma < \gamma_{sn}$, the one-dimensional fast subsystem is bistable, with coexisting spiking and silence regimes. This allows the transition between the silent phase and the active phase of bursting. During the silent phase, the state of the neuron runs η close to the stable bottom branch of the curve of fixed points, while in the active phase the interval between the minimum and maximum iterates of the one-dimensional subsystem $x_{n+1}=F_\alpha(x_n, \gamma)$ lies above the unstable branch of the curve of fixed points. It
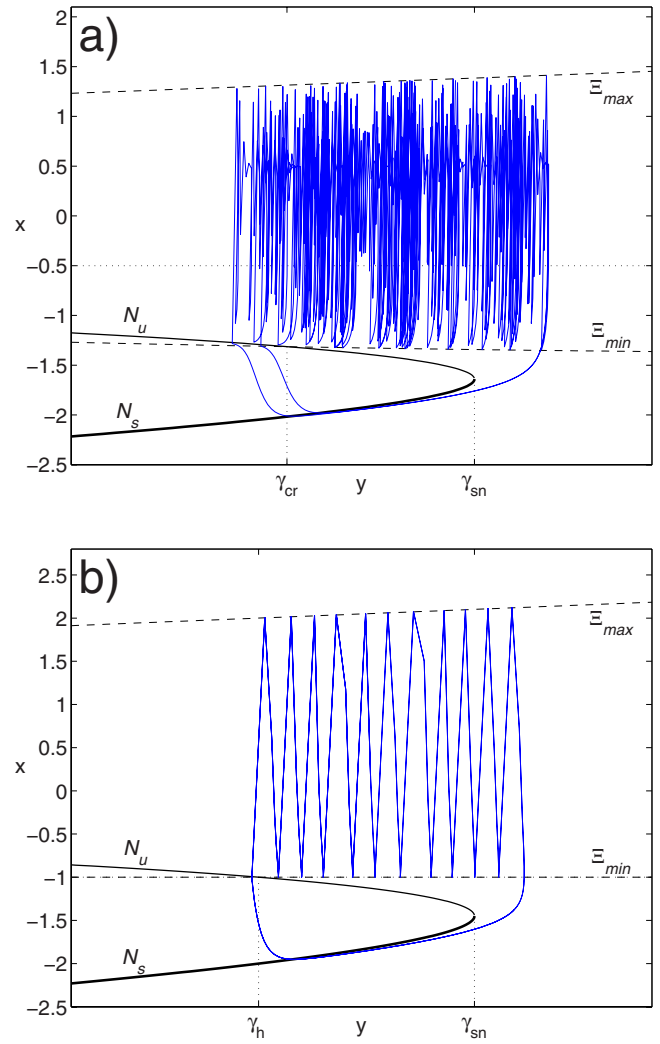
is also necessary for bursting that the position of the slow nullcline is above the stable bottom branch of the fast subsystem nullcline and below the average x value during spiking. Figure 3 shows the orbit in the phase plane of a single neuron of both the chaotic and the nonchaotic maps. Observe that the nonchaotic map presents a periodic bursting trajectory that ends η close to the homoclinic bifurcation at γ_h, while the chaotic map presents irregular bursts that may end well past the external crisis at γ_{cr}.

The condition for bursting can be assessed from a two-parameter bifurcation diagram of the fast subsystem $x_{n+1}=F_\alpha(x_n, \gamma)$ in the (γ, α) plane, as in Fig. 4. In the following we choose for α the values $\alpha=4.15$ in the chaotic case and $\alpha=6$ in the nonchaotic case, both in the middle of the bursting region. Also, unless specified otherwise, the small parameter η will take values $\eta=0.001$ in the chaotic
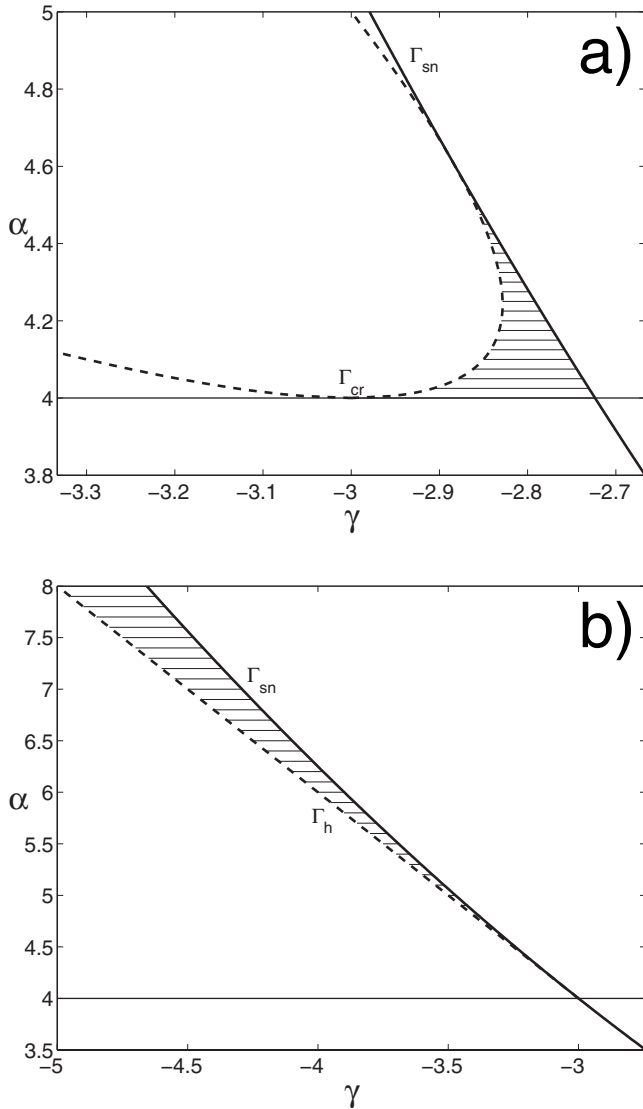
FIG. 4. Two-parameter bifurcation diagram of the single neuron fast subsystem $x_{n+1} = F_\alpha(x_n, \gamma)$ of (a) the chaotic rulkov model and (b) the nonchaotic Rulkov model. The thick solid line Γ_{sn} represents the curve of saddle-node bifurcations. The thick dashed lines Γ_{cr} and Γ_h represent the curves of external crisis and homoclinic bifurcations, respectively. In the shadowed region, bistability exists in the fast variable, and the neuron bursts if σ has an appropriate value.

case and $\eta = 0.002$ in the nonchaotic case, which yield a similar average burst period.

III. BASIC MODES OF SYNCHRONIZATION

When $g_c > 0$ the neurons are coupled and their temporal evolution becomes interdependent. Except for very small values of g_c, this interdependence results in burst synchronization, a process whereby the timing of the bursts of the two neurons becomes strongly correlated. In both the chaotic and nonchaotic case it can be seen that, generally, when synapses are excitatory the neurons synchronize in phase, bursting simultaneously, while inhibitory synapses give rise to an-

tiphase synchronization, with alternating bursts. Examples of the two cases are shown in Fig. 5. Note that bursts are regular in the nonchaotic model and irregular in the chaotic one.

The existence of synchronized states can be explained by the emergence, when coupling grows from zero to a finite value, of a stable attractor in the four-dimensional phase space. This attractor stems from the collapse of the invariant torus defined by the orbits of the uncoupled neurons. A projection of the attractors resulting from in-phase and antiphase synchronization is shown in Fig. 6 for the chaotic model: with inhibitory synapses [Fig. 6(b)], the attractor has two off-diagonal branches that, as the reversal potential increases toward excitatory values, collapse into a single branch covering the whole suprathreshold area [Fig. 6(d)]. An analogous transition takes place in the nonchaotic model, between antiphase and in-phase periodic orbits; in this case, attractors are one-dimensional. In the chaotic case we may characterize the changes in the attractor by measuring its correlation dimension [21]: the dimension of the uncoupled system orbit ($g_c = 0$) is twice that of the isolated neuron ($D = 1.03 \pm 0.02$), while in the coupled system ($g_c > 0$) the dimension deviates from that value, as shown in Fig. 6(a).

However, the relationship between the local properties (such as the correlation dimension) of the attractor and the synchronization regimes is far from trivial and calls for heavy mathematical analysis. Unfortunately, the discontinuous nature of FTM coupling precludes the use of the analytic tools usually employed to explain the origin of these attractors [22] because the two neurons only influence each other through the timing of their transitions across the synaptic threshold θ, and otherwise behave as if isolated. Indeed, when one neuron, for example, neuron 2, has its x variable below θ, neuron 1 follows the isolated neuron equations:

$$x_{n+1,1} = F_\alpha(x_{n,1}, y_{n,1}),$$

$$y_{n+1,1} = y_{n,1} - \eta(x_{n,1} - \sigma). \tag{7}$$

On the other hand, if neuron 2 is above threshold, neuron 1 follows the shifted single-neuron equations:

$$x_{n+1,1} = F_\alpha(x_{n,1}, y_{n,1} - g_c(x_{n,1} - \nu)),$$

$$y_{n+1,1} = y_{n,1} - \eta(x_{n,1} - \sigma). \tag{8}$$

Neuron 2 is affected by neuron 1 in the same way. Thus each neuron may be considered as an isolated system that switches from one dynamic equation to the other depending on the x level of the other neuron. If the threshold θ is such that it lies above the silent branch N_s but below the spiking region delimited by the line of minimum iterates Ξ_{min}, the switching coincides with the alternation between silence and spiking, and this is the key to synchronization of bursts. Observe that the differences between the isolated Eqs. (7) and the shifted Eqs. (8) are negligible at the local level, and therefore features that stem from local properties are mostly insensitive to the coupling and do not explain the origin of the synchronized solutions. For example, Lyapunov exponents, standard indicators of complete synchronization in chaotic systems [22], remain almost unchanged as burst synchronization arises from increasing g_c because they are
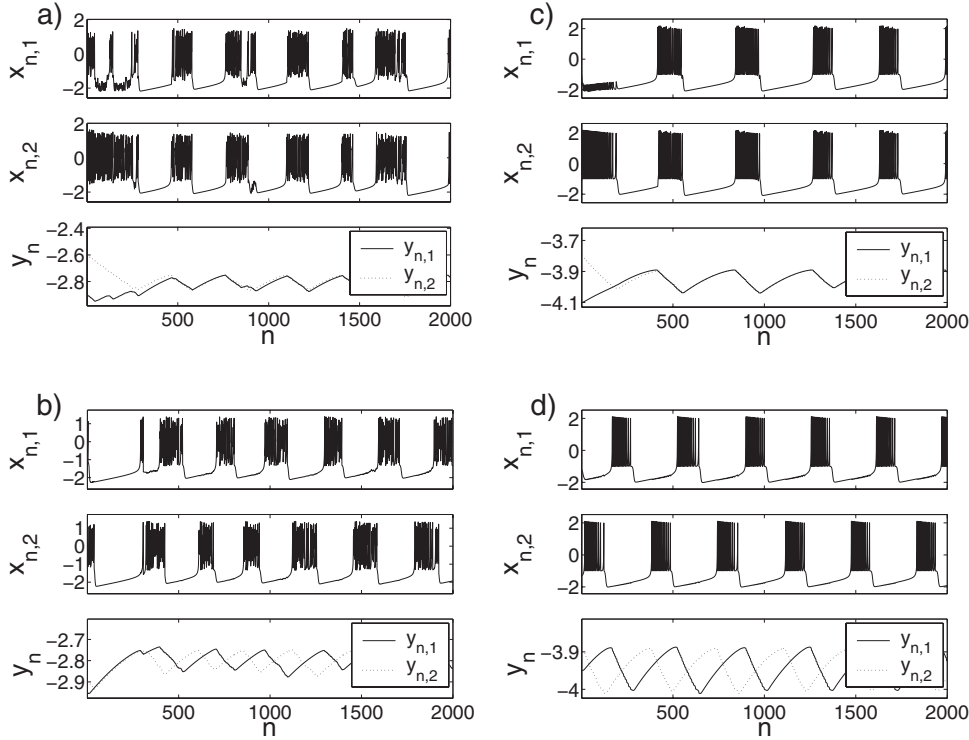
FIG. 5. Time evolution of two coupled neurons, with $g_c=0.1$, $\sigma=-1.25$, and $\theta=0$ in all cases. (a) Chaotic Rulkov neurons with $\nu=1$ (excitatory). (b) Chaotic Rulkov neurons with $\nu=-2$ (inhibitory). (c) Nonchaotic Rulkov neurons with $\nu=1$ (excitatory). (d) Nonchaotic Rulkov neurons with $\nu=-2$ (inhibitory).

dominated by spike dynamics, where the system is most expansive [see Fig. 7(a)]. Thus what they reflect is mostly changes in the duty cycle of bursts, but not in their correlation [Fig. 7(b)].

Since local indices are of little help, the explanation of burst synchronization must come from global differences between the isolated and shifted equations. Such explanation has been given in detail for the Fitzhugh-Nagumo model [18,11], which is a good abstraction of our bursting neurons. A brief summary, as applies to our models, follows, which will give us important clues about the influence of the synaptic parameters upon synchronization. This in turn will be the topic of the next section.

The main difference between the isolated system (7) and the shifted system (8) lies in the position of the nullclines and curves of minimum iterates, and correspondingly of the limiting values γ_{sn} and γ_{cr} or γ_h. This rapid switching of the bursting thresholds is the rationale for the term *fast threshold modulation*. Figure 8 shows both the isolated and shifted phase plane diagram of the chaotic Rulkov model, in the cases of strongly excitatory and strongly inhibitory synapses.

In the excitatory case, the shifted nullclines are to the left of the isolated nullclines. This favors in-phase synchronization as follows (see Fig. 9). Suppose that both neurons are silent and moving rightward along the slow branch N_s of the fast nullcline, with different y values [Fig. 9(a)]. When the neuron with the higher value of y, say neuron 1, reaches $y_{n,1}=\gamma_{sn}$, it jumps up into the spiking regime, above $x=\theta$. This switches the phase plane of the second neuron to the shifted mode, moving its fast nullclines leftwards and either driving it into bursting immediately (if $y_{n,2}>\gamma'_{sn}$ at that moment) or shortening its distance to the saddle-node bifurcation. In the first case, burst initiation occurs synchronously;

in the second, the y gap between both neurons is shortened. Similarly, suppose that both neurons are spiking, also with different y values [Fig. 9(b)]. When the neuron with the lower value of y, say neuron 1, reaches $y_{n,1}=\gamma'_h$ (γ'_{cr} in the chaotic model) it jumps down into the silent regime, below $x=\theta$. This switches the phase plane of the second neuron to the isolated mode, moving its fast nullclines rightwards and either driving it into silence immediately (if $y_{n,2}<\gamma_h$ at that moment, or $y_{n,2}<\gamma_{cr}$ in the chaotic case) or shortening its distance to the homoclinic (or external crisis) bifurcation.

In the inhibitory case, the shifted nullclines are to the right of the isolated nullclines. This favors antiphase synchronization as follows (see Fig. 10). Suppose that both neurons are silent and moving rightward along the slow branch N_s of the fast nullcline, with similar y values [Fig. 10(a)]. When the neuron with the higher value of y, say neuron 1, reaches $y_{n,1}=\gamma_{sn}$, it jumps up into the spiking regime, above $x=\theta$. This switches the phase plane of the second neuron to the shifted mode, moving its fast nullclines, and the saddle-node bifurcation, rightwards. This will delay the bursting of the second neuron. When the first neuron's burst ends [Fig. 10(b)] by reaching $y_{n,1}=\gamma_h$ (γ_{cr} in the chaotic model) it jumps down into the silent regime, below $x=\theta$. This switches the phase plane of the second neuron to the isolated mode, moving its fast nullclines leftwards. Now the second neuron is beyond γ_{sn} and immediately begins spiking, precisely in antiphase with the first.

Other scenarios of in-phase or antiphase synchrony exist depending on neuron parameters. For example, in the antiphase case, the alternation may be due to the silent neuron reaching γ'_{sn} before the other one reaches γ_h or γ_{cr} (intrinsic escape) instead of the other way around (intrinsic release) [18]. For a more detailed discussion the reader is referred to
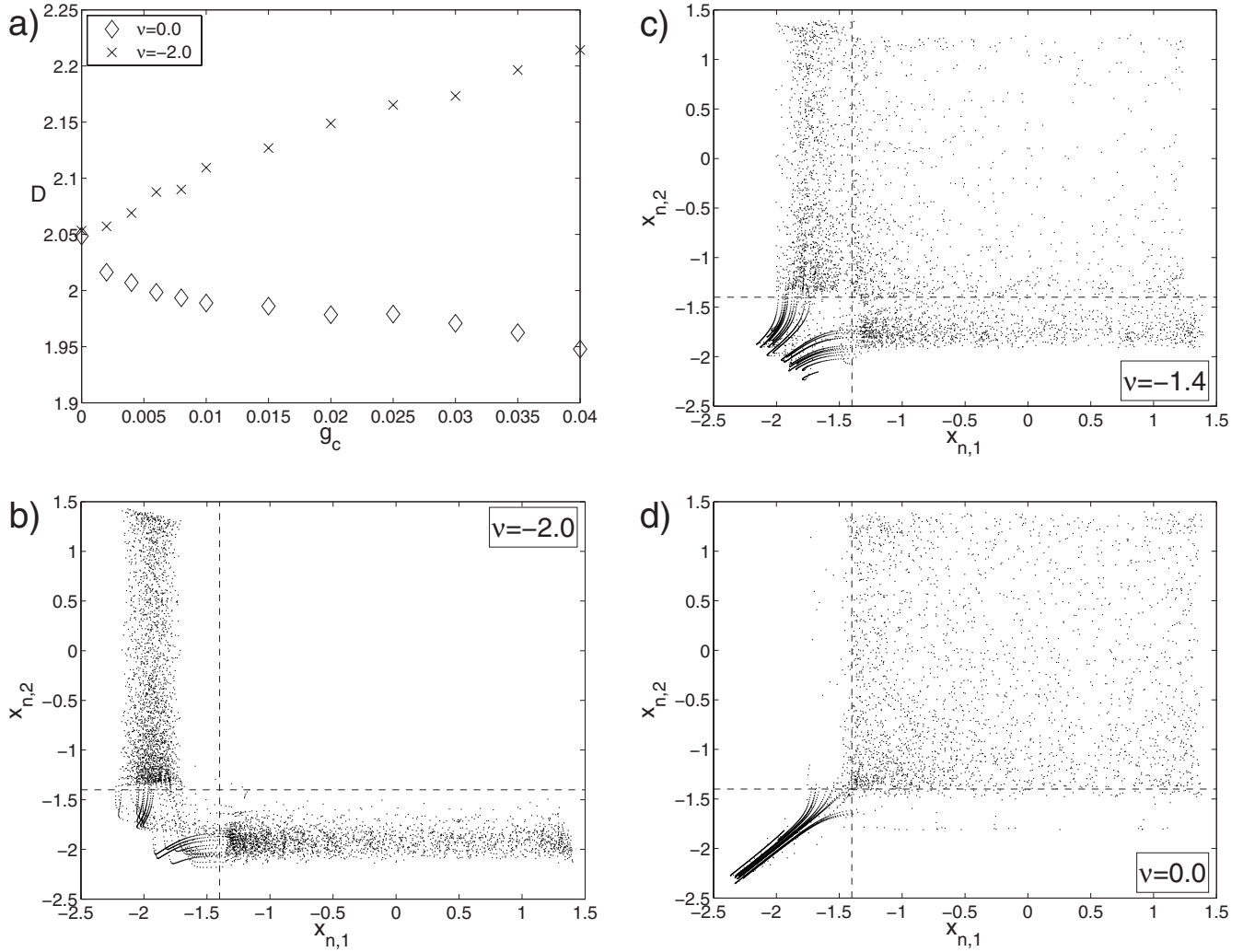
FIG. 6. Simple characterizations of the synchronized dynamics of two chaotic Rulkov neurons. (a) Correlation dimension of the attractor as coupling strength increases from $g_c=0$, for excitatory ($\nu=0.0$) and inhibitory ($\nu=-2.0$) synapses. (b)–(d) Projection of the attractors on the $(x_{n,1},x_{n,2})$ plane for three different synaptic reversal potentials. Dashed lines mark the synaptic threshold ($\theta=-1.4$). Maximal conductance is $g_c=0.1$ in the three cases.

[11,18]. It is easy to see that, in the $\eta\rightarrow0$ limit and with θ above the saddle-node bifurcations but below the curves of minimum iterates, in-phase synchronization is guaranteed if $\gamma_{sn}>\gamma'_{sn}$ and $\gamma_{cr}>\gamma'_{cr}$ (or $\gamma_h>\gamma'_h$). Conversely, antiphase synchronization will set in if $\gamma_{sn}<\gamma'_{sn}$ and $\gamma_{cr}<\gamma'_{cr}$ (or $\gamma_h<\gamma'_h$). In the next section we perform a systematic parameter search to see what values of synaptic strength g_c and reversal potential ν give rise to these conditions, and to explore the less clear-cut and most relevant cases where this is not the case, or where θ is above the curve of minimum iterates $\Xi_{\min}$.

IV. EXHAUSTIVE EXPLORATION OF PARAMETER SPACE

The biological relevance of a neuronal model depends critically on the possibility of relating its variables and parameters to measurable properties of neurons. This is one of the strengths of the fast threshold modulation mecha-

nism, which, despite its extreme simplicity, captures the basic features of fast ionotropic synapses, such as alpha-amino-3-hydroxy-5-methyl-4-isoxazolepropionic acid receptor (AMPA) mediated, in the excitatory case, or type A gamma-aminobutiric acide receptor (GABA$_A$) mediated, in the inhibitory case, in a few meaningful parameters. These are g_c, ν, and θ, and they should be chosen so as to mimic the properties of the particular types of synapses to be modeled. The biological correlate of g_c is the total maximal conductance of the postsynaptic receptor channels, while that of ν is their reversal potential. The dynamics of the system for meaningful ranges of values of these parameters should be explored. The threshold θ is somewhat harder to interpret because it blends together the voltage response and time constant of the synaptic release mechanism. A higher θ corresponds both to a higher presynaptic voltage for neurotransmitter release and to a shorter neurotransmitter binding time. Conversely, low values of θ presuppose longer binding times and lower release thresholds. An exploration of the behavior
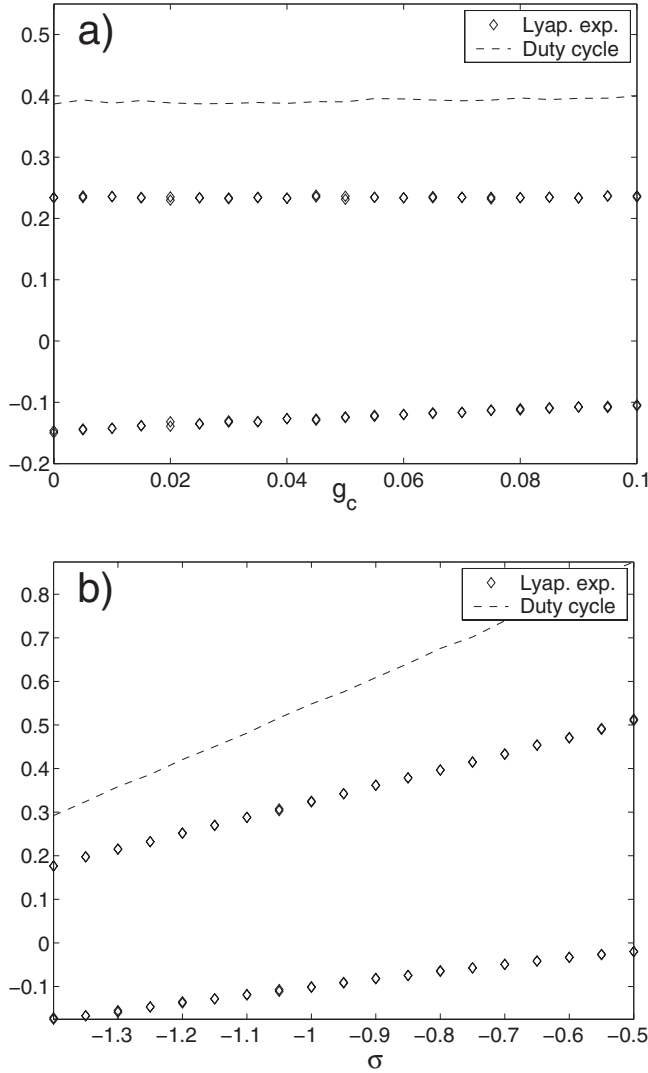
FIG. 7. (a) Dependence of Lyapunov exponents around the attractor as a function of coupling of two chaotic Rulkov neurons. The emergence of a synchronized state as g_c increases is not reflected in the Lyapunov exponents because coupling affects local behavior only very slightly. Other coupling parameters are $\nu=-2$ and $\theta=-1.4$ (results almost identical if $\nu=0$). (b) Further evidence that Lyapunov exponents are not good indicators of synchronization. The exponents in this figure were obtained for two *uncoupled* chaotic neurons ($g_c=0$). Changes in the exponents follow closely the changes in burst duty cycle (dashed) due to variations in excitation σ. This happens because the system is expanding in the spiking intervals, and thus the average expanding rates are higher when spiking takes up a larger fraction of the total time, independently of synchronization.

of the model for different values of θ to assess its precise meaning is also in order.

A. Role of synaptic conductance and reversal potential

Let us first evaluate the effects of different values of g_c, the synaptic conductance, and ν, the reversal potential. In what follows, we will fix the third synaptic parameter, the threshold θ, at $\theta=-1.4$ for the chaotic model and $\theta=-1.1$ for
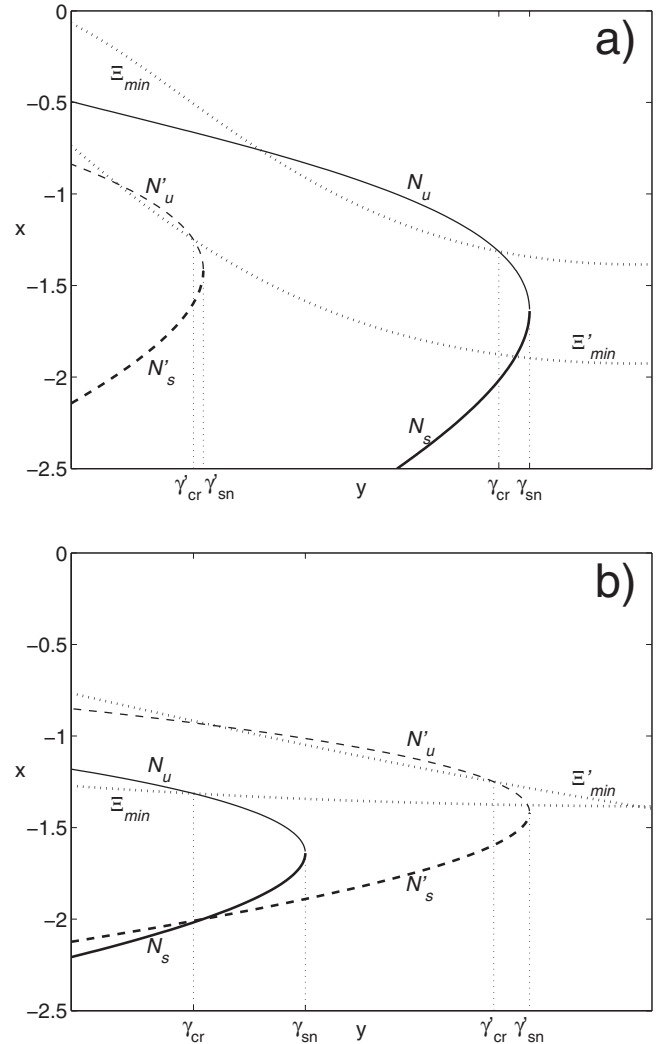

FIG. 8. Phase plane of the chaotic Rulkov model coupled through (a) excitatory ($\nu=1$) and (b) inhibitory ($\nu=-2$), fast threshold modulation synapses. Labels have the same meaning as in Fig. 3(a), with primed versions for the shifted system of Eqs. (8) and unprimed for the isolated system of Eqs. (7). In both cases, $g_c=0.3$. Similar diagrams result from the nonchaotic Rulkov model.

the nonchaotic one. These values make the synapses active along the whole length of the spikes of the presynaptic neuron, and inactive whenever the presynaptic neuron is not spiking. In the next section we will explore the effects of raising the threshold to different levels of depolarization.

Figure 11 depicts, both for the chaotic and the nonchaotic Rulkov models, the positions in the y axis of the saddle-node (Γ'_{sn}) and external crisis (Γ'_{cr}) or homoclinic (Γ'_h) bifurcations of the shifted fast subsystem of Eqs. (8) as a function of g_c, for three different values of ν: one clearly excitatory, one clearly inhibitory, and one in-between. The values of γ_{sn}, γ_{cr}, and γ_h in the isolated system, which are independent of both g_c and ν, are also depicted. We see that in the excitatory case ($\nu=-0.5$) both Γ'_{sn} and Γ'_{cr} (Γ'_h) deviate to the left of γ_{sn} and γ_{cr} (γ_h), respectively. As discussed before, this guarantees in-phase synchronization in the $\eta\to 0$ limit. The opposite happens in the inhibitory case ($\nu=-2$), resulting in antiphase synchronization; but for the intermediate value ($\nu=-1.4$ in
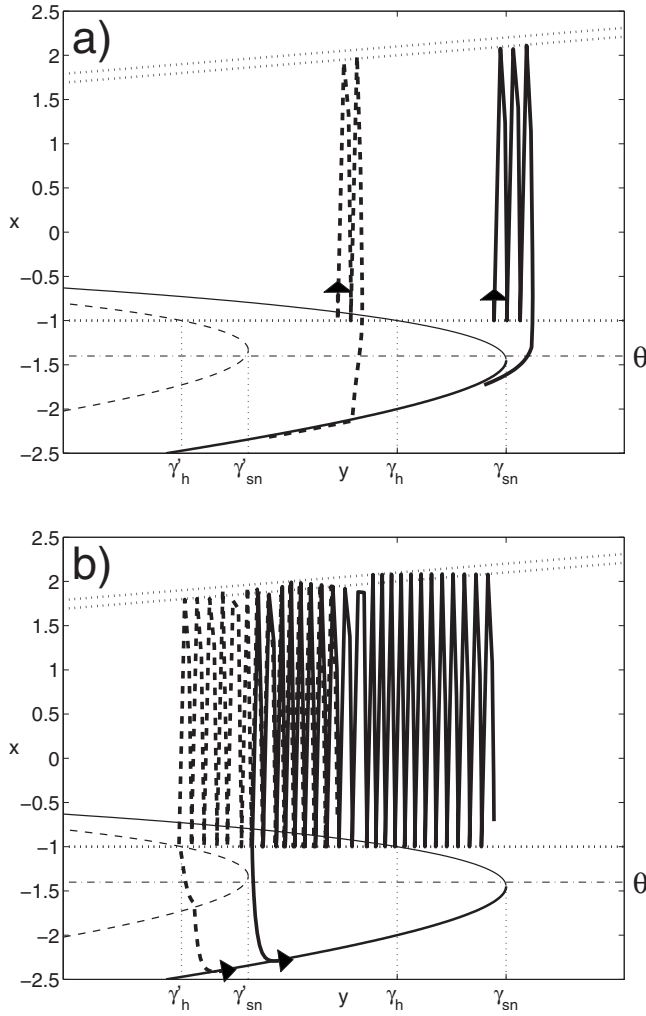
FIG. 9. In-phase synchronization through excitatory ($\nu=1$) FTM synapses in the nonchaotic Rulkov model. (a) When neuron 1 (solid) reaches γ_{sn}, it begins to spike and drives neuron 2 (dashed) into spiking. Thus burst initiation is synchronized. (b) When neuron 2 (dashed) reaches $y=\gamma'_h$ it jumps down into silence, driving neuron 1 (solid) into silence at the same time by shifting its nullclines. Thus burst ending is synchronized. Coupling parameters in this example are $g_c=0.1$ and $\theta=-1.4$. Excitation is $\sigma=-0.9$. A similar mechanism synchronizes bursts in the chaotic Rulkov model.

the chaotic model, $\nu=-1.2$ in the nonchaotic one), Γ'_{sn} is to the left of γ_{sn}, and thus burst initiation favors in-phase synchronization, while Γ'_{cr} (Γ'_h) is to the right of γ_{cr} (γ_h), and burst ending favors antiphase synchronization. As a result, the synchronization mode that in this case finally sets in will be dependent on other parameters, such as σ and θ.

This opens up the interesting possibility of controlling the mode of synchronization without changing the type of synapses, that is, keeping a fixed value of ν while modulating either g_c or σ. This is of great importance in a biological context, where the reversal potential of synaptic connections is mostly fixed and network dynamics must be controlled by modulating either synaptic conductance or background input to neurons. Observe, for example, Fig. 12, which displays one such case in the chaotic Rulkov model. With a reversal potential $\nu=-1.4$ and synaptic strength $g_c=0.1$, we see from
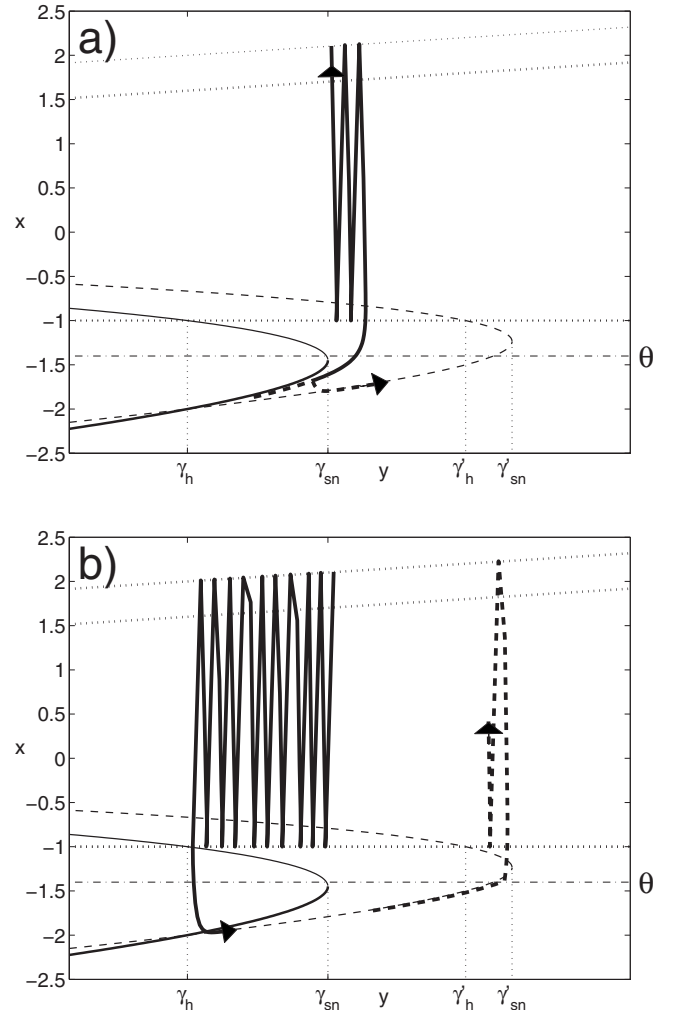
FIG. 10. Antiphase synchronization through inhibitory ($\nu=-2$) FTM synapses in the nonchaotic Rulkov model. (a) When neuron 1 (solid) reaches γ_{sn}, it begins to spike and switches neuron 2 (dashed) to its shifted nullclines. Thus burst initiation of neuron 1 delays burst initiation of neuron 2, favoring antiphase synchronization. (b) When neuron 1 (solid) reaches $y=\gamma_h$ it jumps down into silence; this switches neuron 2 (dashed) to its shifted nullclines and thus immediately releases it for bursting. Therefore the end of bursting in neuron 1 triggers the initiation of a burst in neuron 2. Coupling parameters in this example are $g_c=0.1$ and $\theta=-1.4$. Excitation is $\sigma=-0.9$. A similar mechanism synchronizes bursts in the chaotic Rulkov model.

Fig. 11(a) that the saddle-node bifurcation favors in-phase synchronization ($\gamma'_{sn} < \gamma_{sn}$) but the external crisis bifurcation favors antiphase synchronization ($\gamma'_{cr} > \gamma_{cr}$). When external excitation is high, with $\sigma=-1$ as in Fig. 12(a), the external crisis dominates because, since it takes place in the spiking regime, where x takes on high values, the difference $|x_{n,i}-\sigma|$ is smaller there and, according to the slow subsystem of Eqs. (3), the slow variable spends more time close to that bifurcation than to the saddle-node. The result is mostly antiphase synchronization, with occasional slips due to the irregularity of bursts. On the contrary, when external excitation is low, with $\sigma=-1.5$ as in Fig. 12(b), it is the saddle-node bifurcation that dominates because, since it
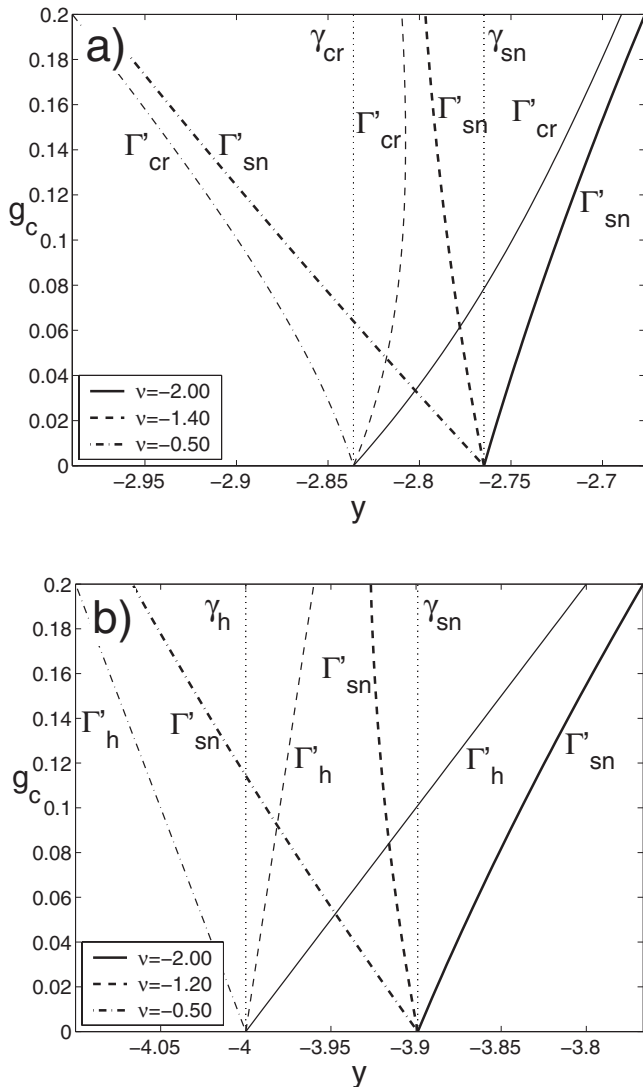
FIG. 11. As a function of g_c, and for three different values of synaptic reversal potential ν: (a) Saddle-node (Γ'_{sn}) and external crisis (Γ'_{cr}) bifurcation curves of the shifted fast subsystem of Eqs. (8) in the chaotic Rulkov model. Vertical dotted lines indicate the position γ_{sn} and γ_{cr} of the isolated neuron bifurcations. (b) Saddle-node (Γ'_{sn}) and homoclinic (Γ'_h) bifurcation curves of the shifted fast subsystem of Eqs. (8) in the nonchaotic Rulkov model. Vertical dotted lines indicate the position γ_{sn} and γ_h of the isolated neuron bifurcations.

takes place at the end of the stable branch of N_s, where x takes on low values, the difference $|x_{n,i} - \sigma|$ is smaller there and, again according to the slow subsystem of Eqs. (3), the slow variable stays longer in this region. The result is mostly in-phase synchronization.

Using intermediate synaptic reversal potentials as in the example above is not a mere curiosity. GABA$_A$ receptor channels, which are selective for chloride ions, have reversal potentials that are, depending on the particular brain system they are located, between -80 and -50 mV. In many cases this potential is very close or slightly above the resting potential of the neuron, and its effect, referred to as *shunting inhibition*, may have a significant role in establishing brain rhythms [23]. In the chaotic Rulkov model, a reversal poten-
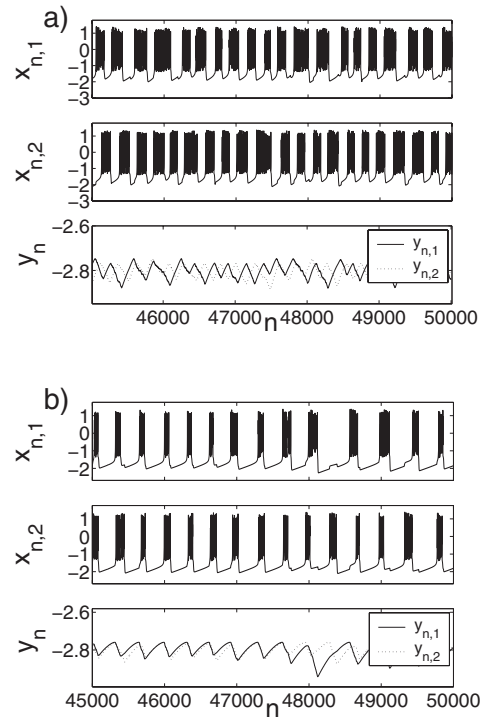

FIG. 12. Different synchronization regimes between two chaotic Rulkov neurons depending on the external excitation. In both cases, synapses have $\nu = -1.4$, $g_c = 0.1$, and $\theta = -1.4$. In (a), $\sigma = -1$ and antiphase synchronization sets in. In (b), $\sigma = -1.5$ and in-phase synchronization dominates. The synchronization regime can be easily recognized by the parallelism or opposition of the slow variables. Apart from this, as it is to be expected, a low value of σ, as in (b), produces sparse bursting while the high value of σ in (a) gives rise to longer bursts.

tial $\nu = -1.4$, as in the above example, plays precisely the same role, since [as can be seen, for example, in Fig. 3(a)] this value is barely above the resting potential defined by the stable branch N_s of the fast nullcline.

Besides, the example above shows that an excitatory, instantaneous synaptic connection may lead to antiphase synchronization. This is contrary to the rule of thumb that excitatory connections favor in-phase bursting while inhibitory connections favor antiphase bursting. In order to explain this further, we shall first state a criterion to classify synapses as excitatory or inhibitory. A synapse is excitatory if it gathers the following two conditions.

E.1. It should produce depolarizing excursions of voltage [excitatory postsynaptic potentials (EPSPs)] upon a resting postsynaptic neuron.

E.2. It should be able to elicit spiking or bursting in the postsynaptic neuron if it is excitable enough (that is, if it is resting but depolarized enough).

Conversely, a synapse will be classified as inhibitory if

I.1. It produces hyperpolarizing excursions of voltage [inhibitory postsynaptic potentials (IPSPs)] upon a resting, sufficiently depolarized postsynaptic neuron.

I.2. It is able to prevent or delay spiking or bursting in an active postsynaptic neuron.

Conditions E.1 and I.1, in our model, depend on the relative position *in the x* axis of the fast nullcline stable branches
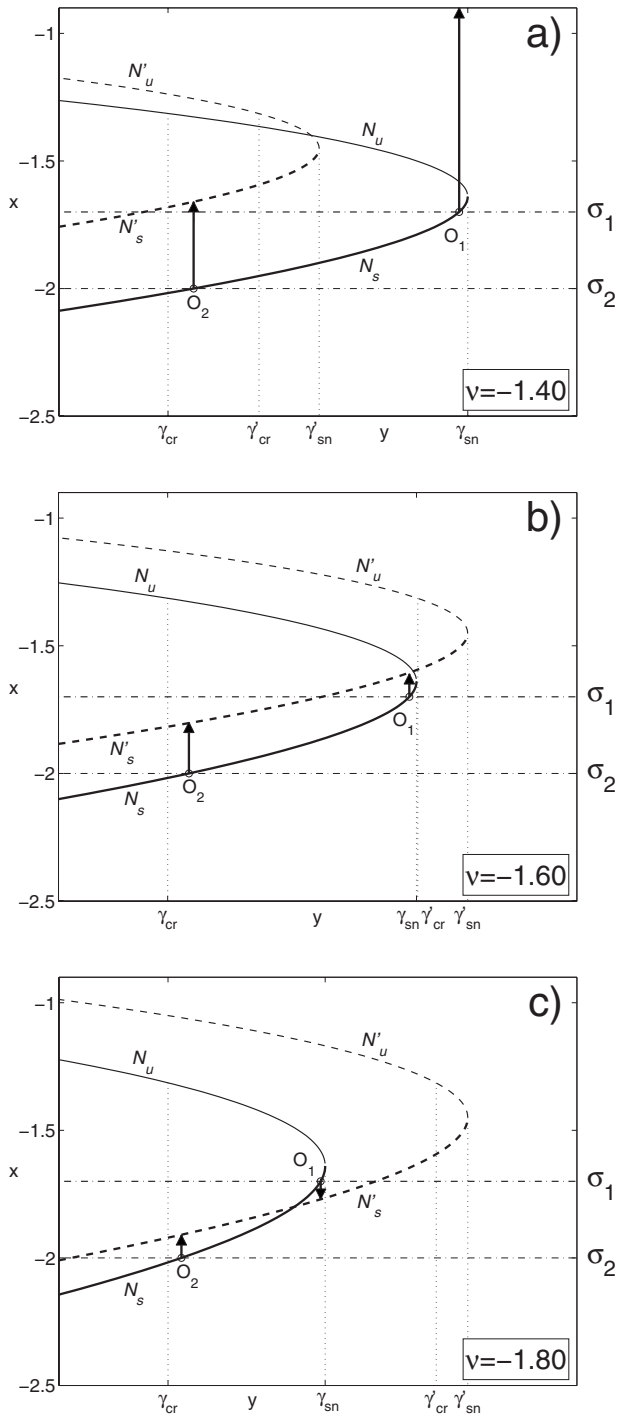
FIG. 13. Effect of synapses on a chaotic Rulkov neuron depending on reversal potential: (a) $\nu=-1.4$; (b) $\nu=-1.6$; and (c) $\nu=-1.8$. Two resting points O_1 and O_2, corresponding to $\sigma_1=-1.7$ (excitable neuron) and $\sigma_2=-2$ (hyperpolarized neuron) are shown in each case. The arrows indicate the jump experienced by the neuron in the $\eta \rightarrow 0$ limit when the synapse is activated. In all cases, $g_c=0.25$. Labels for curves and bifurcation points are the same as in Fig. 8. Similar diagrams result from the nonchaotic model.

N_s and N'_s of the isolated and shifted systems (see Fig. 8). Conditions E.2 and I.2 depend on their relative position *in the y axis*. This is illustrated in Fig. 13. It shows the phase plane diagram of resting neurons, since the values chosen for

σ are always below the saddle-node bifurcation of the isolated neuron. Synapses have maximal conductance $g_c=0.25$, and three different reversal potentials. In Fig. 13(a), the reversal potential is $\nu=-1.4$. The arrows indicate the x excursion that will happen (in the $\eta \rightarrow 0$ limit) when the synapse is activated, at two different resting levels: at σ_1, close to the saddle-node bifurcation, not only will the activation depolarize the neuron (condition E.1), but also a burst will be induced (condition E.2) because the shifted fast nullcline is to the left of the resting point; at σ_2, a depolarizing x excursion happens (condition E.1), but it is limited by N'_s. Anyway the synapse is excitatory because it can generate a burst if the neuron is not too hyperpolarized. On the other hand, in Fig. 13(b), with $\nu=-1.6$, although N'_s is always above N_s and therefore all PSPs are depolarizing (condition E.1), no burst can be elicited by the synapse because all x excursions are limited, due to the horizontal position of N'_s, to the right of N_s. Thus condition E.2 is not met and the synapse is not excitatory, although it cannot be called inhibitory either (being unable to produce any IPSPs, it does not meet condition I.1). Finally, Fig. 13(c) shows a fully inhibitory synapse, with $\nu=-1.8$. It produces hyperpolarizing PSPs in a resting, excitable neuron (condition I.1), and would prevent it from bursting as long as its excitation σ does not go beyond x'_{sn} (condition I.2).

We can turn these observations analytical, at least in the $\eta \rightarrow 0$ limit. First note that according to the fast subsystem part of Eqs. (8), and taking into account Eq. (6), the fixed points x^* of the shifted fast subsystem satisfy

$$\gamma = x^* - f_\alpha(x^*) + g_c(x^* - \nu). \tag{9}$$

Since at the saddle-node the curve of fixed points in the γ-x plane is vertical, the x coordinate x'_{sn} of the bifurcation point must satisfy

$$\left. \frac{\partial \gamma}{\partial x^*} \right|_{x'_{sn}} = 0 \quad \Rightarrow \quad f'_\alpha(x'_{sn}) = 1 + g_c, \tag{10}$$

and, since in all cases, for there to exist a saddle-node bifurcation with growing y, $f''_\alpha(x)>0$ around the saddle-node point, it follows that x'_{sn} grows strictly with g_c. Therefore the saddle-node of the shifted system is always above the saddle-node of the isolated system in the x axis, independent of the particular value of ν or g_c. This means that *condition E.2 will be met if and only if* $\gamma'_{sn} < \gamma_{sn}$, and it will automatically entail E.1. This is a clear characterization of excitatoriness. For example, we see from Fig. 11 that synapses with $\nu=-1.2$ are excitatory for all values of g_c in the nonchaotic model, as are synapses with $\nu=-1.4$ in the chaotic one.

A boundary for excitatoriness may then be defined as the value of ν that makes the Γ'_{sn} bifurcation curve in the g_c-γ plane (see Fig. 11) vertical at $g_c=0$, that is, the value of ν that satisfies

$$\left. \frac{\partial \gamma'_{sn}(g_c, \nu)}{\partial g_c} \right|_{g_c=0} = 0.$$

To obtain this boundary, note that according to Eq. (9), the fast nullcline satisfies

$$\frac{\partial \gamma}{\partial g_c} = [1 - f'_\alpha(x) + g_c]\frac{\partial x}{\partial g_c} + (x - \nu).$$

But at the saddle-node bifurcation, according to Eq. (10), $1 - f'_\alpha(x'_{sn}) + g_c = 0$. Therefore denoting by $x_{sn}(g_c, \nu)$ the value of x at the saddle-node bifurcation, we have that, for any value of g_c,

$$\frac{\partial \gamma'_{sn}(g_c, \nu)}{\partial g_c} = x_{sn}(g_c, \nu) - \nu,$$

and the Γ'_{sn} curve will be vertical in the g_c-γ plane at the point where $x_{sn}(g_c, \nu) = \nu$. Thus, finally, the boundary for excitatoriness is

$$\nu_{exc} = x_{sn},$$

where x_{sn} is the value of x at the saddle-node bifurcation of the isolated fast subsystem. In the particular case of the nonchaotic Rulkov model, $\nu_{exc} = 1 - \sqrt{\alpha} \approx -1.45$ (for $\alpha = 6$). In the chaotic model, the algebraic expression of x_{sn} as a function of α is rather unwieldy; for $\alpha = 4.15$, $\nu_{exc} \approx -1.64$. Whenever $\nu < \nu_{exc}$, synapses will not be excitatory for any value of g_c. For $\nu > \nu_{exc}$, synapses are excitatory at least for low values of g_c. At stronger synaptic conductances the Γ'_{sn} curve may bend rightwards (remember that it is vertical at the point where $x'_{sn} = \nu$) and cross the γ_{sn} vertical line. This change of character with conductance is interesting, but its effect on synchronization properties is mild as we shall see in the next section, where we will compare it to the effect of varying the synaptic threshold θ.

Now that we can easily tell whether a synapse is excitatory, we turn to the issue of synchronization. We can see in Fig. 12 that we cannot aspire to a strict discrimination between in-phase and antiphase behavior in the chaotic Rulkov model, since phase fluctuates between bursts and slips along any single simulation of our system. Even in the nonchaotic model, and although for clear-cut situations such as that of Figs. 5(c) and 5(d) we may find global attractors corresponding to one of the two regimes, for the intermediate synaptic values we are interested in, chaotic trajectories are the norm and attractors seem extremely hard to analyze as a function of parameters. We turn instead to numeric calculation of the cross-correlation between the x trajectories of both neurons for different initial conditions. A positive average cross-correlation should indicate in-phase bursting and negative antiphase. To verify this, we perform the calculation with $g_c = 0$ (that is, two uncoupled neurons); average cross-correlation in this case is close to zero, and we obtain confidence intervals around it to test for the significance of our results.

Figure 14 shows the cross-correlations obtained with both the chaotic and nonchaotic models as a function of external excitation σ, for fixed $g_c = 0.2$ and different values of ν right above the excitatory boundary ν_{exc}. As we predicted from the bifurcation curves in Fig. 11 and phase-plane analysis of the FTM mechanism, for a fixed reversal potential low values of σ favor in-phase synchronization (positive cross-correlation) but, as σ grows, the dephasing effect of burst ending gains importance and the regime switches to antiphase (negative
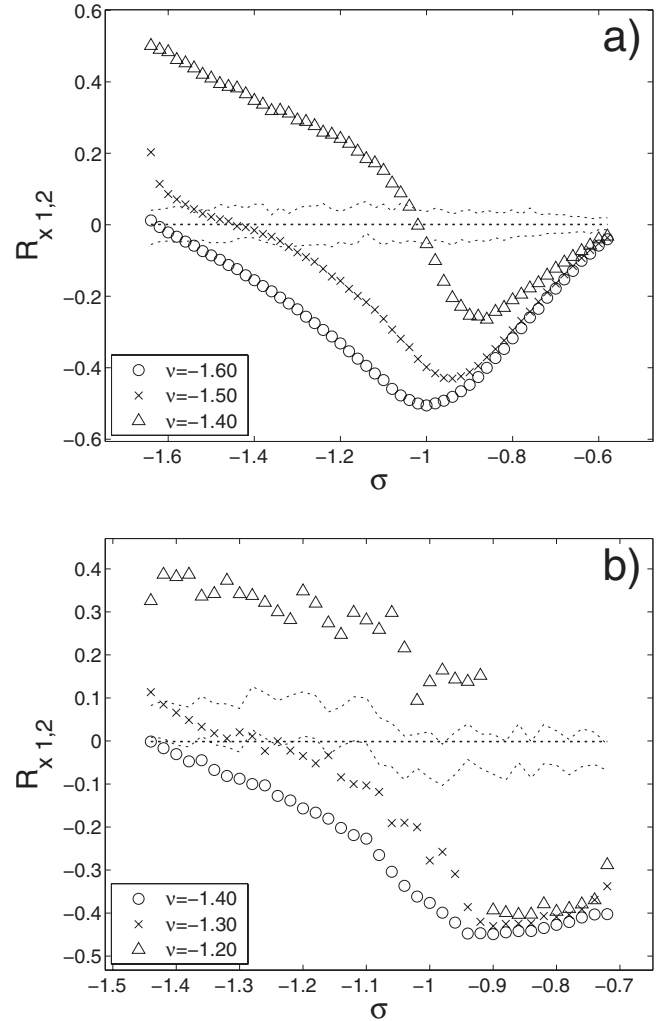

FIG. 14. Average cross-correlation of $x_{n,1}$ and $x_{n,2}$ of 50 trials of length $n_{max} = 50\,000$, as a function of excitation σ for different values of synaptic threshold ν. The dotted lines represent the 95% confidence interval of significance against the null hypothesis of uncoupled neurons. (a) Chaotic Rulkov model, with $g_c = 0.2$ and $\theta = -1.4$. (b) Nonchaotic Rulkov model, with $g_c = 0.2$ and $\theta = -1.1$. Note the sharp change in cross-correlation in the nonchaotic model at $\sigma = -0.9$ when $\nu = -1.2$.

cross-correlation values). The switching is gradual in the chaotic model, but may turn out to be rather sharp in the nonchaotic one. For example, with $\nu = -1.2$ synchronization changes abruptly at $\sigma \approx -0.92$ when the speed along N'_s becomes fast enough to stabilize an antiphase orbit that never falls onto N_s. We can thus control the regime of the system with very small changes in external excitation. The reason why cross-correlation grows again for very high σ is that bursts achieve duty cycles above 50%, producing overlaps that drive the cross-correlation toward positive values even if burst initiation continues to be alternating.

A graphical comparison of the modulating possibilities of the two models can be seen in Fig. 15, where the cross-correlation between $x_{n,1}$ and $x_{n,2}$ as a function of both σ and ν is represented by means of contour plots. The thick contour corresponds to zero cross-correlation and we can chart horizontal (fixed ν) lines to assess the variation of the synchro-
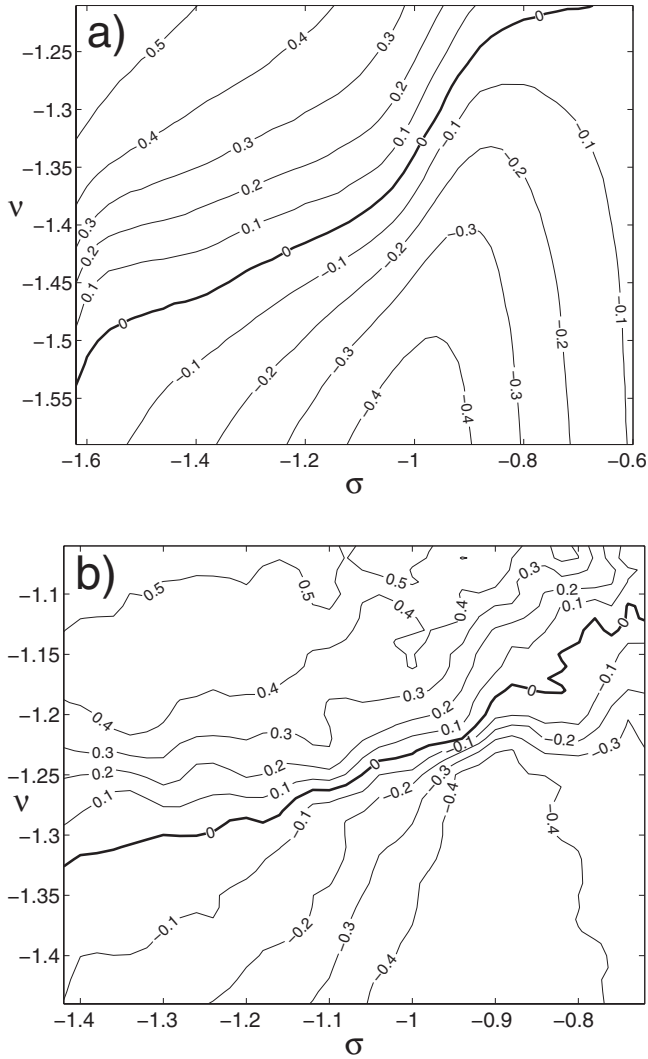
FIG. 15. Contours of constant cross-correlation of $x_{n,1}$ and $x_{n,2}$ in the σ-ν plane, for (a) the chaotic Rulkov model, and (b) for the nonchaotic Rulkov model. In both cases $g_c=0.1$. The contours were obtained from averages of 50 trials of length $n_{max}=50\,000$ in a grid of resolution $\Delta\nu=0.04$ and $\Delta\sigma=0.02$. The thick contour highlights zero cross-correlation.

FIG. 16. Contours of constant cross-correlation of $x_{n,1}$ and $x_{n,2}$ in (a) the θ-ν plane, with $g_c=0.1$, and (b) the g_c-ν plane, with $\theta=0$, for the chaotic Rulkov model. The contours were obtained from averages of 50 trials of length $n_{max}=50\,000$ in a grid of resolution $\Delta\nu=0.04$, $\Delta\theta=0.1$, and $\Delta g_c=0.01$. In both figures $\sigma=-1.5$. The thick contour highlights zero cross-correlation. Notice that the g_c axis in (b) is inverted for easy comparison with the effects of θ in (a).

nization regime with external excitation σ. Notice that reversals of synchronization only occur in a well-defined range of values of ν above the excitation threshold ν_{exc}. Also note that contours are tightly packed in the nonchaotic model, inidicating a sharper transition.

B. Role of the synaptic threshold

We now turn to investigate the effects of varying θ. As θ raises from below the spike reset level, the neurons switch from remaining steadily coupled during bursts to an intermittent coupling at the spiking frequency, to fully uncoupled when θ goes beyond the maximum x value of spikes. Thus we may conjecture that increases in θ will have an effect similar to decreases in g_c. This is indeed the case from the point of view of burst synchronization, as shown in Fig. 16 for the chaotic Rulkov model. The mild ascending slope of
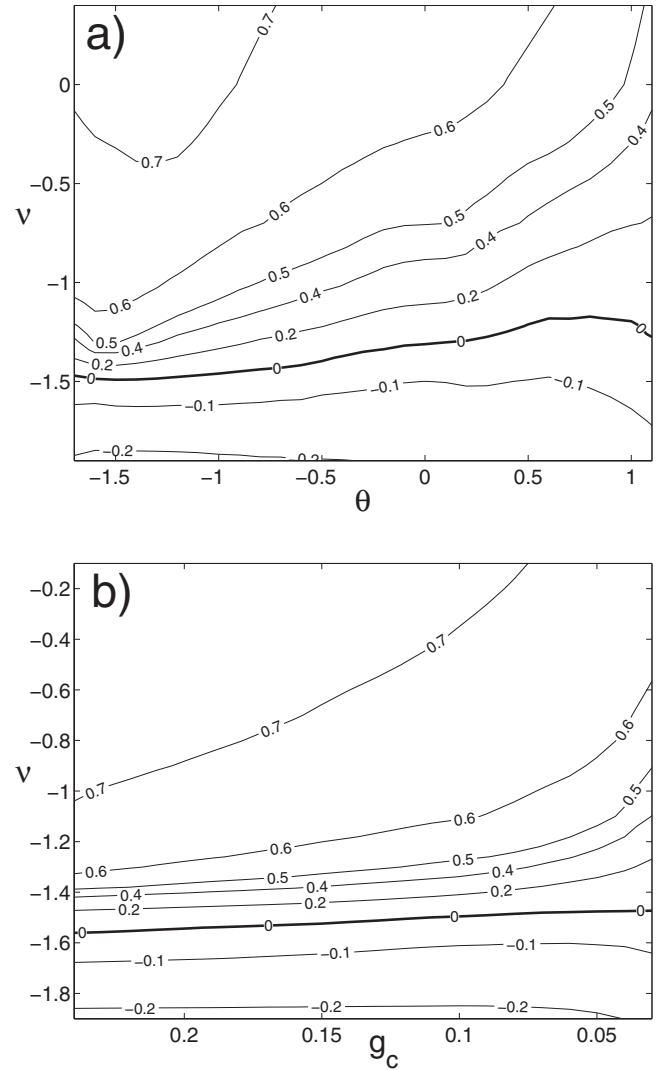
the zero cross-correlation contour in both the θ-ν and g_c-ν diagrams indicates that, for reversal potentials between -1.5 and -1.4 (which, as we saw previously, may produce in-phase or antiphase synchronization when modulated by σ), weakening the synapses (that is, either increasing θ or decreasing g_c) has a very mild desynchronizing effect. More noticeable is the fact that, while clearly excitatory ($\nu>-1$) or inhibitory ($\nu<-1.7$) synapses retain their synchronizing power up to very low values of g_c (contours remain mostly parallel), they turn ineffective very rapidly as θ raises toward the spike maximum (note the diverging contours in the $\theta-\nu$ plane as θ grows; maximum spike x value is around $x=1.4$).

At any rate, the effect of g_c and θ in controlling burst synchronization for a fixed ν is very mild compared to the

effect of σ. This may strike one as surprising in the light of the Γ'_{sn} and Γ'_{cr} curves of Fig. 11(a), where we can see that the distance in the y axis between the isolated and shifted system bifurcations is strongly dependent on g_c. But this affects mostly the rate at which the system reaches the synchronized regime [11]; whether this regime is synchronized in-phase or antiphase depends rather on the dominance of burst initiation over burst ending or vice versa, and this is controlled by σ.

In spite of their similar effects on burst synchronization, there is a clear difference in the dynamics of coupling using a weak g_c or a high synaptic threshold θ: in the latter case, each neuron is subject to a pulsed perturbation at the spike frequency during each of the bursts of the presynaptic neuron, while in the former there is only one time scale for the perturbation, namely the average burst period. The high frequency perturbation does not affect burst synchronization because resonances responsible for burst initiation are dominated by the slow subsystem [24] and burst response at the spiking frequency is highly damped. For this reason we only observe an average reduction in synaptic effectiveness comparable to a decrease in g_c; but we shall presently see that the high frequency perturbation does have an effect on *spike* synchronization in the in-phase synchronized bursting regime *of the nonchaotic Rulkov model*.

Figure 17(a) shows the cross-correlation between $x_{n,1}$ and $x_{n,2}$ in the nonchaotic Rulkov model as a function of ν and θ. It should be compared with Fig. 16(a), which is its equivalent in the chaotic model. We have chosen to use a gray level diagram instead of contours here because the irregularity of the nonchaotic case turns the contour plot unreadable. Indeed, although the antiphase bursting region (below $\nu=-1.35$, approximately) is rather uniform with values of cross-correlation around -0.5, the in-phase bursting region (above $\nu=-1.25$, approximately), with average values of cross-correlation around 0.5, is bespeckled with white spots representing a cross-correlation of 1. In these spots, the neurons synchronize not only their bursts but also their spikes: they achieve complete synchronization. On the other hand, in the gray region surrounding these spots, bursts are synchronized in-phase, but spikes are antiphase, producing a significantly positive but lower cross-correlation. The difference between the two cases is shown in Figs. 17(b) and 17(c). A rather surprising fact is that tiny variations in the synaptic threshold θ (from $\theta=0.30$ to 0.33 in our example) are enough to switch the system from one mode to the other. It is also interesting to note that spike synchronization is relatively rare: the white areas in Fig. 17(a) fill up a small portion of parameter space. Let us briefly explain why.

Consider just the fast subsystem of Eqs. (2) along the spiking orbits. We try to find, for fixed values γ_1 and γ_2, the basin of attraction of the synchronized orbit in the $(x_{n,1}, x_{n,2})$ plane. Since in the cases under study bursts are synchronized, we will suppose $\gamma_1=\gamma_2=\gamma$ first; we will discuss afterwards what happens when γ_1 and γ_2 differ. Because all spikes take off from $x=-1$, it is enough to investigate whether an orbit starting at $(x_{n,1}, x_{n,2})=(-1, x_0)$, with $-1 < x_0 < \alpha+\gamma$, will or will not end up in synchrony. According to the reset mechanism of Eq. (5), synchrony will ensue if, at some point, both neurons cross the threshold $x=0$ in the
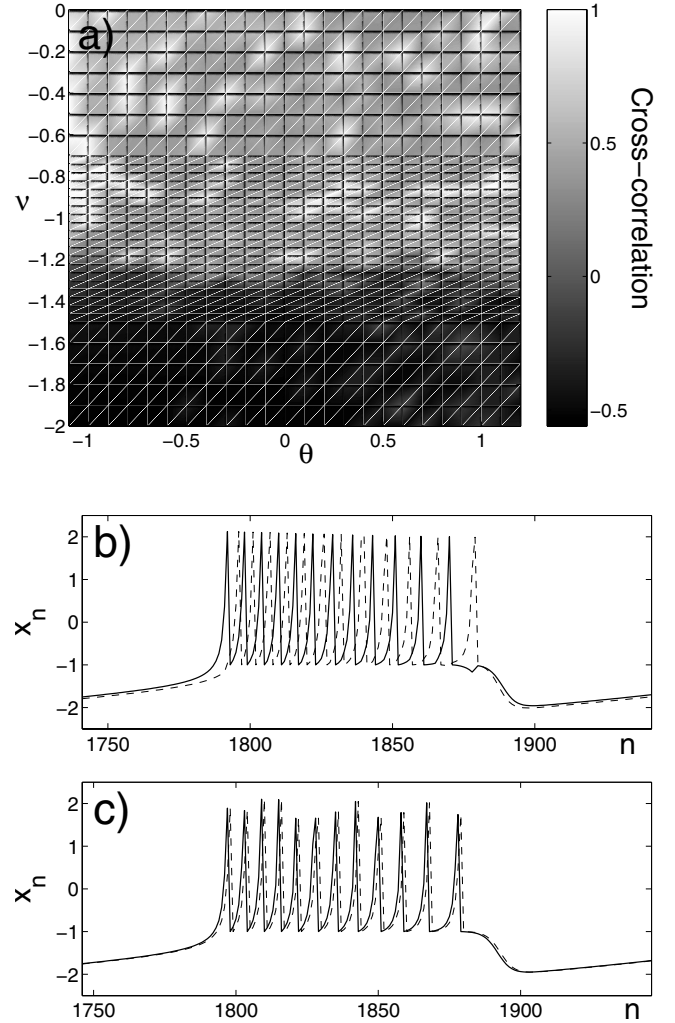

FIG. 17. (a) Cross-correlation of $x_{n,1}$ and $x_{n,2}$ in the nonchaotic Rulkov model as a function of ν and θ, for $g_c=0.25$ and $\sigma=-1$. Values of cross-correlation were obtained from averages of 50 trials of length $n_{\max}=50\,000$ in a grid of resolution $\Delta\nu=0.04$ and $\Delta\theta=0.1$. (b) Evolution of $x_{n,1}$ (solid line) and $x_{n,2}$ (dashed) at $\nu=-0.6$, $g_c=0.25$, $\sigma=-1$, and $\theta=0.33$: bursting is in-phase, spiking is antiphase inside each burst. (c) Same as in (b), but for $\theta=0.30$: both bursts and spikes are synchronized in-phase, corresponding to a white spot of correlation 1 in (a). The orbit of neuron 2 has been shifted one sample in order to visualize it (otherwise, both orbits would be coincident).

same iteration; the expanding nature of the return map below threshold forbids the possibility of synchronizing by gradual contraction of the orbits. If no interaction existed, or, equivalently, if $\theta > \alpha+\gamma$, it is evident that the condition for synchronization would be

$$-1 \le x_0 < F_\alpha^{-(n_\gamma-1)}(0,\gamma), \qquad (11)$$

where $n_\gamma=\min\{n; F^n(-1,\gamma) > 0\}$. In the other extreme case, when $\theta < -1$, the same rule is valid using the shifted fast map $F_{\alpha,\text{shifted}}(x,\gamma)=F_\alpha(x,\gamma)-g_c(x-\nu)$. The basins are thus intervals between -1 and some higher value. In the intermediate cases where $-1 < \theta < \alpha+\gamma$ we cannot derive a simple formula for the basin: depending on g_c, ν, and the position of
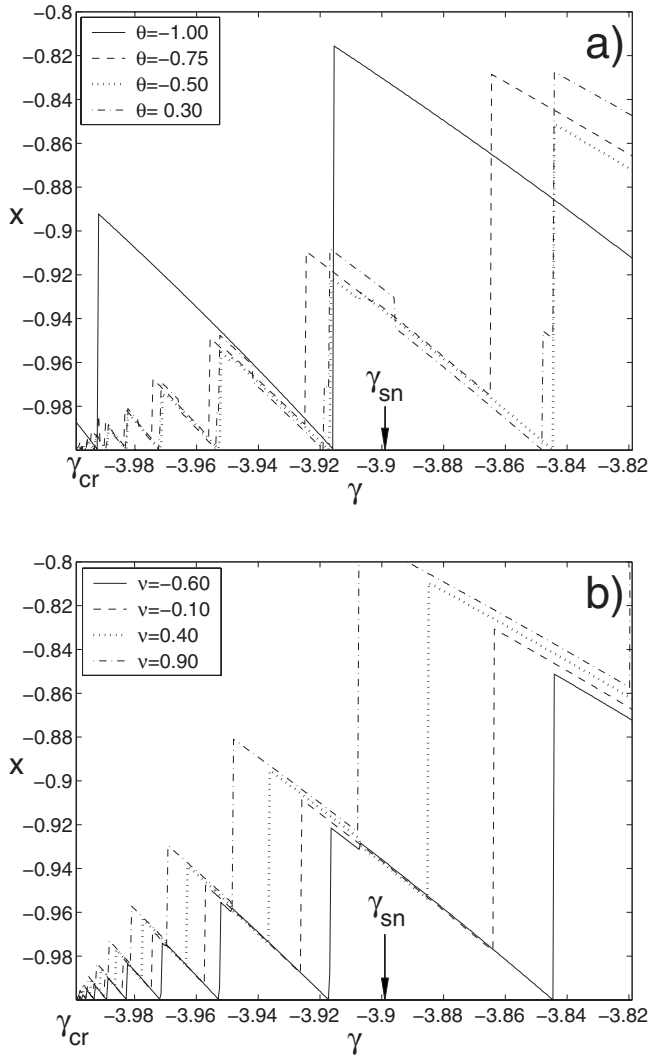
FIG. 18. Boundary of the basin of attraction of synchronized spike orbits in the fast subsystem of the nonchaotic Rulkov model as a function of $\gamma_1 = \gamma_2 = \gamma$. The basins are intervals starting at $x = -1$ and ending at the depicted profiles. (a) Dependence of the basin on the synaptic threshold θ. Other parameters are $\nu = -0.6$ and $g_c = 0.25$. (b) Dependence of the basin on the synaptic reversal potential ν. Other parameters are $\theta = -0.5$ and $g_c = 0.25$. Note that the solid line in (b) is the same as the dotted line in (a).

the threshold, the orbit starting at $x = -1$ may even surpass the orbit beginning at $x = x_0 > -1$ if at some point the first is below threshold, the second is above, and ν is higher than both; thus the basin need not be an interval, and analytical expressions become unwieldy. Numerical calculation instead is easy, and we find indeed that for the values of g_c and ν of interest ($0 \leq g_c < 0.3$, $-1 < \nu < 1$) basins continue to be intervals, at least down to a precision of $\Delta x = 0.0001$. Figure 18 shows how the basins change with γ, for different values of θ and ν. The sawtooth-shaped basin profiles are to be expected from the form of Eq. (11). For example, the discontinuities of the $\theta = -1$ profile of Fig. 18(a) correspond to the values of γ where $F_\alpha^{n\gamma}(0, \gamma) = 0$ and therefore the period of the spike cycle changes in one unit. At those points, a period-adding bifurcation takes place, and the basin becomes the single point $x = -1$ because even the slightest difference in

the point of departure will translate into a different number of iterations to return to $x = -1$ and will prevent synchronization. With $\theta > -1$ profiles become more irregular and dented due to further discontinuities introduced by the crossings of the synaptic threshold. The dependence of the profiles on parameters is complex and we just intend to highlight that both θ and ν have a strong effect upon the position and shape of the basins.

In the full system with synchronized bursts, synchronization of spikes is decided at the beginning of the burst. Both neurons shoot up into spiking somewhere past the saddle-node $y = \gamma_{sn}$, which has been marked in Fig. 18. One of them will spike first, and when it resets to $x_{n,i} = -1$ (or after a few spikes, if the other neuron lags significantly), the other neuron will be at some point along the spiking interval. For spike synchronization to ensue, this point should be in the basins depicted in Fig. 18. Note that the basins occupy a small interval close to $x = -1$, and thus spike synchronization is rare. It is further complicated by the effect of mismatches between $y_{n,1}$ and $y_{n,2}$, which naturally arise along the orbits of the full system. If $\gamma_1 \neq \gamma_2$, the discontinuities in the basins prove fatal for synchronization of spikes because they correspond, as we have explained, to changes in the spike period. We can see this in Fig. 19(a): in the first burst spikes have synchronized and the system is very close to full synchronization, except for a slight mismatch in y; the second burst begins with synchronized spikes, but halfway through it the neurons switch to antiphase because one of them (that of the solid line) adds one iteration to its spike cycle before the other does. Just as we have depicted the basins of spike synchronization for $\gamma_1 = \gamma_2$, we can do the same for $\gamma_2 - \gamma_1 = \Delta\gamma > 0$ to observe the deletereous effect of γ mismatch on synchronization basins [Fig. 19(b)]. When there is a mismatch, the end of each tooth of the saw does not coincide with the beginning of the next one, and there are whole intervals of y along the burst where even if both neurons begin at $x = -1$ at the same time they will not synchronize just due to the fact that they have a different number of iterations per spike.

Needless to say that the entry point of bursting along the γ line, which is determinant to decide whether spikes will synchronize, is strongly dependent on the finite value of η and on the position of the slow nullcline $x = \sigma$. Thus, all in all, spike synchronization is a complex process where all parameters have a say. For our purposes it is enough to stress that θ can control spike synchronization independently of g_c, and in this regard raising or lowering the synaptic threshold is not merely equivalent to weakening or strengthening the synapse.

Spike synchronization is exclusive of the nonchaotic model. In fact, we cannot even extrapolate the heuristic analysis we have performed to continuous-time equivalents of the Rulkov map: in continuous time, no period-adding bifurcations take place and the basins for synchronization do not have the characteristic sawtooth profile. In continuous-time systems, the effects of synaptic threshold on spike synchronization can be predicted by the well-known technique of phase-response curves [25].
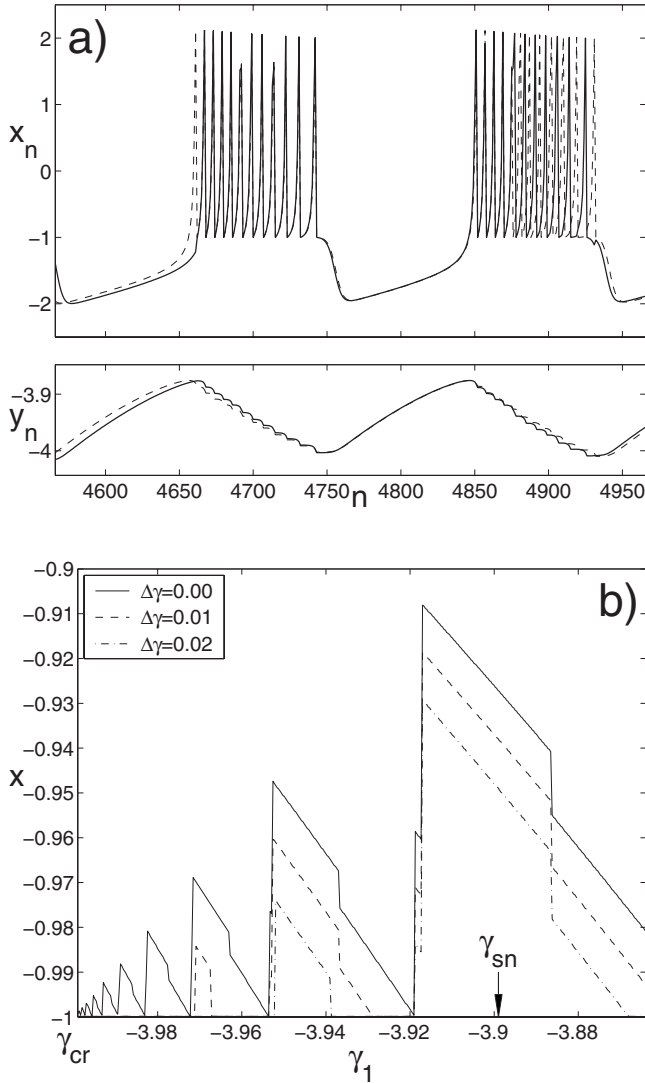
FIG. 19. (a) Top: evolution of $x_{n,1}$ (solid line) and $x_{n,2}$ (dashed); bottom: evolution of $y_{n,1}$ (solid line) and $y_{n,2}$ (dashed), along a bursting orbit with $\nu=-0.6$, $g_c=0.25$, $\sigma=-1$, and $\theta=0.5$. In the first burst spikes have synchronized and the system is close to full synchronization, but during the second burst the slight mismatch between $y_{n,1}$ and $y_{n,2}$ is enough to destroy it. (b) Boundaries of the basin of attraction of synchronized spike orbits in the fast subsystem as a function of γ_1 for different values of $\Delta\gamma=\gamma_2-\gamma_1$ and the same parameters as in (a). When $\Delta\gamma>0$, the teeth of the profile are separated by gaps where spike synchronization is impossible.

FIG. 20. Raster plots of the bursting patterns in a ring of $N=32$ nonchaotic Rulkov neurons. In all cases $\alpha=6$, $\eta=0.002$, $g_c=0.1$, and $\theta=-1.1$. External excitation σ is $\sigma=-1.2$ for $n=1,\ldots,10\,000$ and $\sigma=-0.8$ for $n=10\,001,\ldots,20\,000$. (a) $\nu=0.0$, in-phase burst synchronization. (b) $\nu=-1.2$, switch between in-phase and antiphase synchronization. (c) $\nu=-2.0$, antiphase synchronization.

V. CONCLUSION AND DISCUSSION

In this paper we have investigated the synchronization regimes of two map-based bursters coupled through fast threshold modulation. We have examined how synchronization depends on coupling parameters such as the reversal potential of the synaptic channels, the maximal conductance of the synapses and the synaptic threshold, and explained the results with heuristic arguments based on examination of the phase plane and fast-slow decomposition.

We have seen that changes in the synaptic threshold θ are mostly equivalent to changes in synaptic conductance because of the averaging effect of the slow process of bursting.
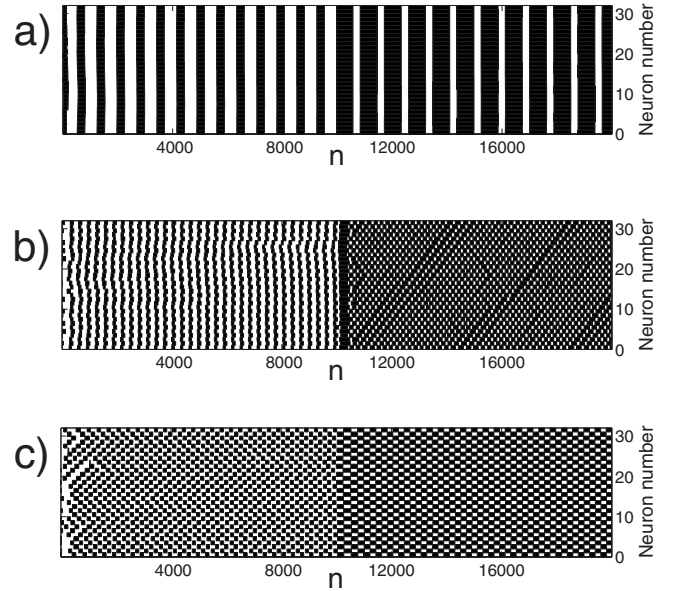
The only exception is for spike synchronization, which, at any rate, is only an artifact of the discretization implied in the map-based nonchaotic model and has no direct bearing on realistic models. The interchangeability of θ and g_c is good for modeling, since θ is a phenomenological parameter, hard to derive from biophysical measurements, while g_c is more easily identifiable.

More interestingly, we have found that the burst synchronization regimes arising from synaptic connections with mildly excitatory reversal potentials are sensitive to modulatory signals such as the steady external excitation of the neurons. Two chaotic or nonchaotic Rulkov neurons bursting in phase may be switched to antiphase synchronization by a steady increase in σ. It is interesting to see how this reflects on the dynamics of a network of neurons. In Fig. 20 three raster plots are presented with the bursting pattern of a ring of $N=32$ nonchaotic Rulkov neurons. Each neuron in the ring is coupled to its two nearest neighbors. To be precise, the equations of the system are

$$x_{n+1,i} = F_\alpha(x_{n,i}, y_{n,i} + \beta_{n,i}),$$

$$y_{n+1,i} = y_{n,i} - \eta(x_{n,i} - \sigma),$$

for $i=0,\ldots,N-1$, with

$$\beta_{n,i} = -g_c[H(x_{n,i-1}-\theta)(x_{n,i-1}-\nu) + H(x_{n,i+1}-\theta)(x_{n,i+1}-\nu)],$$

where indices $i+1$ and $i-1$ must be understood modulo N. Each raster is made up of 20 000 iterations; along the first half external modulation is $\sigma=-1.2$, while in the second half $\sigma=-0.8$. In Fig. 20(a), the reversal potential of the synapses is $\nu=0$. These are fully excitatory synapses and regardless of
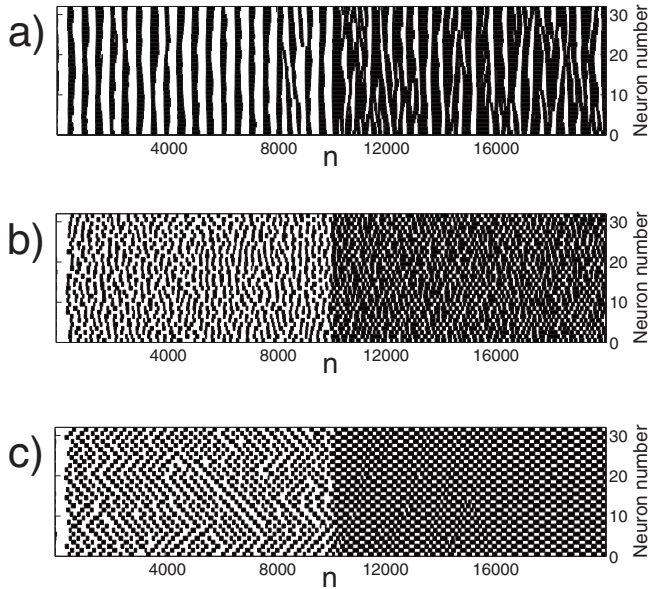
FIG. 21. Raster plots of the bursting patterns in a ring of $N=32$ chaotic Rulkov neurons. In all cases, $\alpha=4.15$, $\eta=0.001$, $g_c=0.1$, and $\theta=-1.4$. External excitation σ is $\sigma=-1.4$ for $n=1,\dots,10\,000$ and $\sigma=-1.0$ for $n=10\,001,\dots,20\,000$. (a) $\nu=0.0$, in-phase burst synchronization with occasional slips and propagation of activity. (b) $\nu=-1.45$, switch between predominantly in-phase behavior (striped pattern) and predominantly antiphase behavior (checkered pattern). (c) $\nu=-2.0$, antiphase propagation in the first half and antiphase synchronization in the second.

σ the ring synchronizes in-phase; the higher σ merely enlarges the duty cycle of bursts. In Fig. 20(c), $\nu=-2$ is fully inhibitory and, again regardless of σ, neurons synchronize in antiphase; but at $\nu=-1.2$ which, just as with $\nu=-1.4$ in the chaotic model, is only mildly excitatory, the change in external excitation results in a full change of the network pattern, from simultaneous to alternating bursts. This was to be predicted in the light of the cross-correlation profile of Fig. 14(b) for $\nu=-1.2$: a sharp change from positive to negative correlation takes place at around $\sigma=-0.9$; very small changes in σ can have a strong effect on network synchronization if synapses are involved with reversal potentials close to shunting.

In the case of the chaotic model the extrapolation from two-neuron behavior to ring dynamics is not so obvious. As we see in Fig. 21(a), with fully excitatory synapses synchronization is in-phase independently of external excitation, but occasional readjustments with propagation of activity happen unpredictably due to the irregularity of the individual bursts. The readjustments seem to be more frequent when excitation is higher. This can be explained by the fact that, as we know, high σ implies dominance of the external crisis bifurcation over the saddle-node bifurcation in determining burst length. Since, for bursts synchronized in-phase, the irregularity is due exclusively to burst ending through the external crisis, a higher σ produces more irregular bursts and translates into more frequent slips of synchronization in the network. In Fig. 21(b) we see the case of a mildly excitatory synapse, with $\nu=-1.45$. We gather from Fig. 14(a) that at this synaptic level synchronization should be mostly in-phase for low ex-
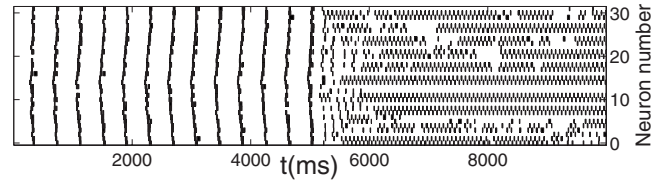

FIG. 22. Raster plot of the bursting patterns in a ring of $N=32$ neurons with Hodgkin-Huxley dynamics connected by shunting ($GABA_A$) synapses to their nearest neighbors. The model and parameters are as in [26], except that the $GABA_A$ synapses have a reversal potential of -60 mV. External excitation is $I=0.05$ $\mu A/cm^2$ during the first half of the simulation and $I=0.35$ $\mu A/cm^2$ during the second half. The network switches from a dominantly in-phase to a dominantly antiphase pattern.

citation and antiphase for high excitation. The pattern is not as clear-cut as in the equivalent nonchaotic case of Fig. 20(b), but indeed with low σ bursts occur predominantly in stripes, while an alternating, checkered pattern covers most of the high σ area of activity. Finally Fig. 20(c) shows the interesting case of fully inhibitory synapses. As expected, regardless of σ, neighboring neurons will not burst in-phase, but this does not entail antiphase synchronization: for low σ, propagating patterns appear. If we look at vertical cuts of these patterns, we can see that they consist of neurons synchronizing in-phase not with their next-nearest neighbor, as antiphase synchronization would require, but with the neurons located two positions away. In other words, the duty cycle of bursts is low enough to accommodate three bursts in sequence, and this produces the waves we see across the ring. This phenomenon happens also, and due to the same reasons, in the nonchaotic model for an excitation lower than that of Fig. 20 (not shown).

The simple map-based models of our choice have allowed us to gain insight into their dynamics by means of phase plane analysis, but the implications we have derived for burst synchronization extend to elaborate burster models that share a similar bursting mechanism. As an example Fig. 22 shows the activity in a ring of bursters modeled with Hodgkin-Huxley equations that include four different intrinsic currents and $GABA_A$ synapses with first order dynamics [26]. By switching the level of current injected into the neurons, without any change in synaptic or intrinsic properties, the network switches from an in-phase to an antiphase regime. Similar effects may result from modulating signals or shifts in background excitatory inputs, and shunting synapses may thus provide a mechanism for rapid, flexible control of the rhythms generated by networks.

We finish with a comment on the implications for general network structures. The relationship between the topology of a network of bursters and its patterns of activity is a topic of interest for the understanding of systems as diverse as thalamic neurons during periods of sleep or drowsiness [4], dopaminergic neurons in the midbrain [27], pancreatic β cells [3], and central pattern generator neurons. In a recent work we have shown [10] how for direct, linear inhibitory coupling between neurons, the spectral properties of the network graph correctly predict the bursting patterns. Here we merely point out that, although we cannot extend the analyti-
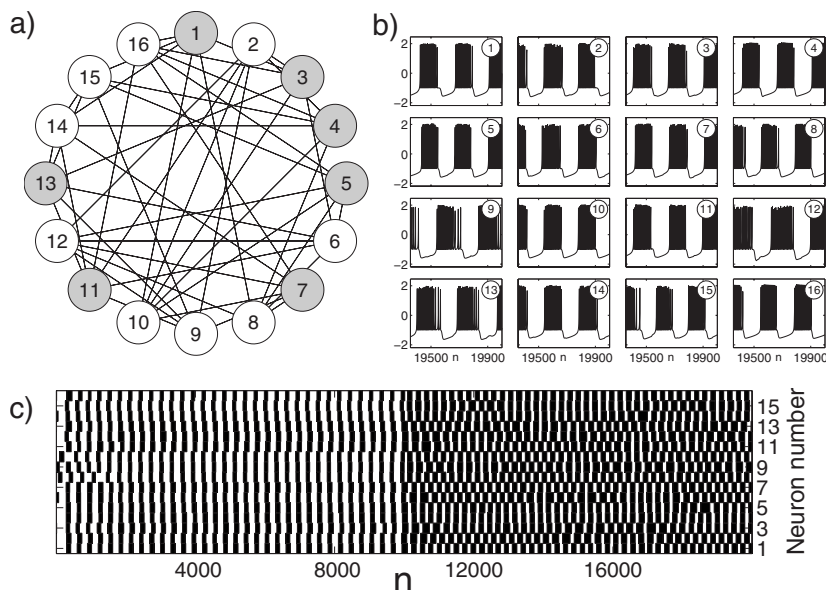
FIG. 23. (a) Structure of a small regular network of 16 nonchaotic Rulkov neurons. Each neuron has six incoming synapses. Neurons have been divided in two groups (white and gray) according to the sign of their components in the dominant eigenvector of the adjacency matrix of the graph. (b) Activity in the network, corresponding to the last part of the raster in (c). We see neurons 1, 3, 4, 5, 7, and 11 firing in synchrony, and also 2, 6, 8, 10, 14, 15, and 16. They correspond to the two clusters shown in (a). Neurons 9, 12, and 13 are undecided between both clusters. (c) Raster plot of bursts in the network. In this simulation, $\sigma=-1.2$ for $n=1,\dots,10\,000$ and $\sigma=-0.8$ for $n=10\,001,\dots,20\,000$. In the first part, the whole network is synchronized approximately in-phase; in the second, neurons split in clusters that closely follow the division in two groups shown in (a), with frequent slips and readjustments. Other parameters are $\alpha=6$, $\eta=0.002$, $g_c=0.033$, and $\theta=-1.05$.

cal techniques used there to FTM coupling, the same properties, and to be precise, the components of the dominant (most negative) eigenvalue of the adjacency matrix of the network graph, determine the clusters of neurons that fire in synchrony *when coupling is such as to produce antiphase bursting in two coupled neurons*. This means that we can control the pattern of activity in a general network by modulation of σ, just as we did in a ring. Figure 23(a) shows a 16-neuron symmetric random network of degree 6. The raster in Fig. 23(c) shows how an increase in σ switches the network from in-phase synchronization to a pattern of bursts where two clusters of neurons that tend to fire in synchrony can be determined that split the network along the same lines as the sign of the dominant eigenvector of the adjacency matrix. This is exactly what happens with direct, linear inhibitory coupling, although in that case one of the clusters

remains silent [10]. We can see that the synchrony is not perfect and there are frequent slips of some neurons that readjust the bursting pattern; the neurons that slip more frequently are those with smallest eigenvector components (12, 13, 2, and 9). A close-up of the bursts can be seen in Fig. 23(b).

[1] W. Singer, Neuron **24**, 49 (1999).
[2] P. J. Uhlhaas and W. Singer, Neuron **52**, 155 (2006).
[3] J. Aguirre, E. Mosekilde, and M. A. F. Sanjuán, Phys. Rev. E **69**, 041910 (2004).
[4] M. Steriade and D. A. McCormick, Science **262**, 679 (1993).
[5] M. Bevan, P. Magill, D. Terman, J. Bolam, and C. Wilson, Trends Neurosci. **25**, 525 (2002).
[6] E. Marder and D. Bucher, Curr. Biol. **11**, R986 (2001).
[7] E. M. Izhikevich, Int. J. Bifurcation Chaos Appl. Sci. Eng. **10**, 1171 (2000).
[8] *Bursting: The Genesis of Rhythm in the Nervous System*, edited by S. Coombes and P. C. Bressloff (World Scientific, New York, 2005).
[9] G. Tanaka, B. Ibarz, M. A. F. Sanjuán, and K. Aihara, Chaos **16**, 013113 (2006).
[10] B. Ibarz, J. M. Casado, M. A. F. Sanjuán, and K. Aihara, Phys. Rev. E **75**, 041911 (2007).
[11] D. Somers and N. Kopell, Biol. Cybern. **68**, 393 (1993).
[12] L. M. Pecora and T. L. Carroll, Phys. Rev. Lett. **80**, 2109 (1998).

[13] J. Rubin and D. Terman, in *Handbook of Dynamical Systems*, edited by B. Fiedler (North-Holland, Amsterdam, 2002), Vol. 2, pp. 93–146.

[14] J. Best, A. Borisyuk, J. Rubin, D. Terman, and M. Wechselberger, SIAM J. Appl. Dyn. Syst. **4**, 1107 (2005).

[15] G. de Vries, in *Bursting: The Genesis of Rhythm in the Nervous System*, edited by S. Coombes and P. Bressloff (World Scientific, Singapore, 2005), pp. 223–242.

[16] N. F. Rulkov, Phys. Rev. Lett. **86**, 183 (2001).

[17] N. F. Rulkov, Phys. Rev. E **65**, 041922 (2002).

[18] F. K. Skinner, N. Kopell, and E. Marder, J. Comput. Neurosci. **1**, 69 (1994).

[19] M. Courbage, V. I. Nekorkin, and L. V. Vdovin, Chaos **17**, 043109 (2007).

[20] G. de Vries, Phys. Rev. E **64**, 051914 (2001).

[21] P. Grassberger and I. Procaccia, Phys. Rev. Lett. **50**, 346 (1983).

[22] A. Pikovsky, M. Rosenblum, and J. Kurths, *Synchronization: A Universal Concept in Nonlinear Sciences*, Cambridge Nonlinear Science Series Volume 12 (Cambridge University Press, New York, 2003).

[23] I. Vida, M. Bartos, and P. Jonas, Neuron **49**, 107 (2006).

[24] B. Ibarz, G. Tanaka, M. A. F. Sanjuán, and K. Aihara, Phys. Rev. E **75**, 041902 (2007).

[25] B. S. Gutkin, B. G. Ermentrout, and A. D. Reyes, J. Neurophysiol. **94**, 1623 (2005).

[26] M. Bazhenov, I. Timofeev, M. Steriade, and T. J. Sejnowski, J. Neurophysiol. **79**, 2730 (1998).

[27] W. Schultz, J. Neurophysiol. **80**, 1 (1998).